NEAR-INFRARED CAMERA AND MULTI-OBJECT SPECTROMETER OBSERVATIONS OF THE HUBBLE DEEP FIELD: OBSERVATIONS, DATA REDUCTION, AND GALAXY PHOTOMETRY

RODGER I. THOMPSON
Steward Observatory, University of Arizona, Tucson, AZ 85721

LISA J. STORRIE-LOMBARDI AND RAY J. WEYMANN
Carnegie Observatories, 813 Santa Barbara Street, Pasadena, CA 91101

AND

MARCIA J. RIEKE, GLENN SCHNEIDER, ELIZABETH STOBIE, AND DYER LYTLE
Steward Observatory, University of Arizona, Tucson, AZ 85721

ABSTRACT

This paper presents data obtained during the NICMOS Guaranteed Time Observations of a portion of the Hubble Deep Field. The data are in a catalog format similar to the publication of the original WFPC2 Hubble Deep Field program (Williams et al.). The catalog contains 342 objects in a $49''.1 \times 48''.4$ subfield of the total observed field, 235 of which are considered coincident with objects in the WFPC2 catalog. The 3 σ signal-to-noise ratio level is at an aperture AB magnitude of approximately 28.8 at 1.6 μm. The catalog sources, listed in order of right ascension, are selected to satisfy a limiting signal-to-noise ratio criterion of greater than or equal to 2.5. This introduces a few false detections into the catalog, and users should take careful note of the completeness and reliability levels for the catalog discussed in §§ 9 and 10. The catalog also contains a test parameter indicating the results of half-catalog tests and the degree of coincidence with the original WFPC2 catalog.

Key words: cosmology: observations — galaxies: fundamental parameters

1. INTRODUCTION

Deep observations with the Near-Infrared Camera and Multi-Object Spectrometer (NICMOS), devoted to understanding the nature of galaxy formation and evolution along with information on cosmological parameters, have always been an important aspect of the NICMOS Instrument Development Team (IDT) program since its inception in 1984. After the WFPC2 Hubble Deep Field (HDF) program in late 1995, it became obvious that observations at longer wavelengths would greatly enhance the value of the existing data in addition to satisfying the original intent of deep observations. The smaller field of view of the NICMOS instrument made it necessary to choose between deep observations of a portion of the HDF and a survey of the entire HDF at a brighter limiting magnitude. With the advent of the HDF, there existed a large disparity between the depth of the HDF and the depth of observations at near-infrared wavelengths (Connolly et al. 1997). Since the majority of objects that might be at redshifts unobservable with WFPC2 were expected to be relatively faint, the IDT decided to conduct a limited spatial survey to the faintest possible magnitude. The results of a NICMOS General Observer HDF survey program (Dickinson et al. 1997) will provide coverage over the entire HDF.

The NICMOS HDF program consists of 127 orbits out of a total of 553 orbits for the entire GTO program. Table 1 shows the distribution of orbits between the two filters and two grisms. An additional two orbits were dedicated to confirmation of guide star acquisition. Although the bulk of the orbits are dedicated to imaging, the large comoving volume for line observations available to the grisms is very appealing. The small number of grism orbits shown in Table 1 were intended as test cases to see if more GTO orbits should be transferred to this program. In order to

expedite the delivery of image data to the community at large, we have not concentrated on the reduction of the grism data, and it is not presented in this publication. The grism data will be published in subsequent papers. As discussed below, the grism observations, however, significantly influenced the choice of the field for NICMOS imaging observations.

As with the Williams et al. (1996) paper, the purpose of this publication is a presentation of the data and analysis techniques rather than a discussion of the scientific content of the data. Future papers will discuss several implications of the new data. In the following we present the rationale for the observation methods, the methods for image production and source extraction, the catalog, and a discussion of the quality of the data in terms of signal-to-noise ratio, completeness, and reliability. Note that all magnitudes quoted in this paper are in the AB system.

2. FIELD SELECTION

The decision to devote part of the observational time to grism observations limited field choices to regions of the HDF that are not dominated by large bright foreground galaxies. The slitless dispersed spectra of these galaxies would overlap large areas of the field of view and reduce the number of spectral observations of fainter galaxies. Although some information on high-redshift objects was available at the time of field selection, no effort was made to bias the field position to include the largest number of high-redshift sources.

The Space Telescope Science Institute decision to schedule the NICMOS HDF observations during the Camera 3 campaign in January of 1998 determined the acceptable range of roll orientations. This time period was not part of the continuous viewing zone (CVZ) opportunity period;

TABLE 1

Basic Parameters of the NICMOS Hubble Deep Field

R.A. (J2000.0)	Decl. (J2000.0)	Orient (deg)	Total Field (arcsec)	F110W (orbits)	F160W (orbits)	G096 (orbits)	G141 (orbits)
12 36 45.129	+62 12 15.55	261.851	57.87 × 61.34	49	49	12	15

Note.—Units of right ascension are hours, minutes, and seconds, and units of declination are degrees, arcminutes, and arcseconds.

however, it did offer a larger fraction of truly dark observing time. Given these constraints, a field located roughly at the center of the WFPC2 chip 4 field offered the best observational opportunities. The J2000.0 center position is $12^h36^m45^s.129$, $+62°12'15''.55$. There is a relatively bright star (AB_H of approximately 22.1 mag) near the center that provides an excellent fiducial location for the grism observations. The final orient of $261°.851$ is the result of fine tuning to obtain the best possible guide star orientation.

3. FILTER AND CAMERA SELECTION

3.1. Camera Selection

All of the NICMOS HDF data in this paper are from Camera 3. The wide field format of Camera 3 made it the obvious choice for HDF observations. The campaign also utilized Cameras 1 and 2 with the same integration parameters as Camera 3, but they were not in focus during operation. Parallel observation of these cameras with Camera 3 prevented the occurrence of the faint artifacts, termed bars, which occur when the autoflush and imaging output timing patterns overlap. Similar integration parameters for all cameras prevents the parallel cameras from defaulting into the autoflush pattern. The data from these cameras may be useful for background characterization but are not analyzed in this publication.

3.2. Filter Selection

The observations employed two imaging filters for Camera 3, F110W and F160W centered at 1.1 and 1.6 μm, respectively. By careful design, the F160W spans the lowest background spectral region available to NICMOS. This is the minimum between the scattered zodiacal emission that decreases with wavelength and the thermal emission from the warm *Hubble Space Telescope* (*HST*) mirrors that

increases with wavelength. Both of these emissions were lower than expected prior to the HDF observations. The second filter covers a shorter wavelength over a rather broad bandwidth. This filter provides a second color between the F814W WFPC2 filter and the NICMOS F160W filter. The addition of this filter provides an important discriminator between high-redshift star-forming galaxies, which will have blue infrared colors, and lower redshift galaxies with large amounts of dust extinction, which will have red infrared colors. Although very useful for all objects, the extra filter is particularly important for objects detected only in the NICMOS bands. Figure 1 displays the normalized detectivity for the NICMOS filters. These plots include all of the color-dependent terms of the detectivity, including the detector quantum efficiency. The rapidly changing indices of refraction for most optical coating materials in the 1 μm region account for the complicated shape of the F110W filter.

4. OBSERVATIONAL STRATEGY

The preflight decision to devote 49 orbits to each imaging filter and 27 orbits to grism spectroscopy set the parameters for the observing strategy. The 49 orbits are based on a 7 × 7 grid of positions, and the grism orbits employ three different roll angle positions to help remove confusion from overlapping spectra. There are three separate integrations in each orbit to ensure that any problems encountered did not necessarily compromise all of the data during the orbit. Before the observations it appeared that the sky background would be the dominant noise source after about 900 s of integration. The lower than expected sky brightness, however, reduced the sky noise below the read noise for this integration time.

4.1. Detector Sampling Sequence

Since there are no bright sources in the HDF, the logarithmic NICMOS sampling sequences, designed to handle high dynamic range images, are inappropriate. Those sequences add amplifier glow noise with several short time integrations near the beginning of the exposures. Good cosmic-ray rejection, on the other hand, requires a sufficient number of samples to establish an accurate signal after any cosmic-ray–affected samples are rejected. The HDF integrations utilize the SPARS64 sampling sequence that has evenly spaced 64 s sample times after the first three short integration samples. The integrations have a NSAMP value of 17, which produces a total integration time of 896 s. Three of these integrations fill an orbit. The total number of integrations in each filter is then 147 integrations of 896 s in each filter for a total of 1.31712×10^5 s or 36.5 hr of observing time per filter.

4.2. Field Coverage

Several factors influenced the choice of field size. The basic purpose of the NICMOS HDF program is deep
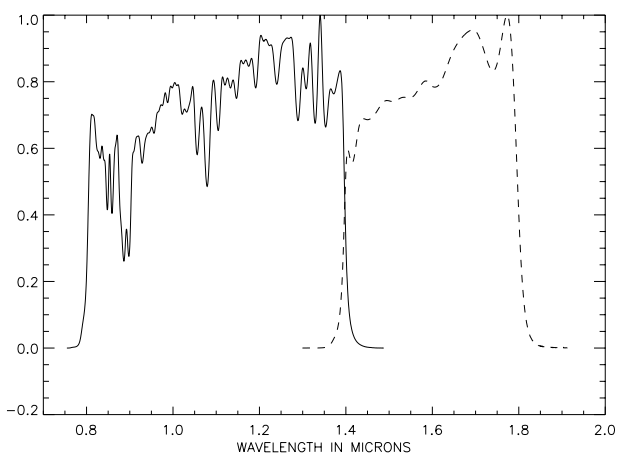

Fig. 1.—Normalized total filter response functions for the NICMOS F160W and F110W filters. These response functions include all of the color-dependent terms including the detector quantum efficiency.

observations. This requirement favors very small or no dithers away from the field center. Accurate background subtraction requires many offsets large enough to ensure that most pixels have the majority of their observations off of detectable objects. Spatial cosmic-ray rejection and image resolution enhancement require at least 1 pixel and fractional pixel offsets, respectively.

The pattern of observation positions on the sky is a combination of a small three-point dither pattern during each orbit and a larger 7×7 raster pattern that covered the 49 orbits. The dither pattern is a three-position spiral dither with a step size of $0''.408$, roughly 2 Camera 3 pixels. The x- and y-spacings of the orbit-to-orbit raster are $0''.918$ and $1''.523$, respectively, which are 4.5 and 7.5 Camera 3 pixels. The interorbit moves were accomplished with target offsets from the original center position. The basic purpose of the raster was to move the field of view sufficiently that any single pixel had the majority of its integrations with no observable source present.

4.3. Pointing Accuracy

Owing to the paucity of bright stars in the HDF region and the roll constraints during the observational time period, we were not able to utilize two FGS guide stars. This situation led to the possibility of roll errors in position about the location of the single guide star. Real time frequent updates of the gyro bias levels by *HST* Missions Operations Support Engineering Systems (MOSES) mitigated this problem. Data provided by the MOSES team (C. Conner 1998, private communication from the Missions Operations Support Engineering Systems) indicated that the positional errors for all orbits used in this paper were less than 0.2 NICMOS Camera 3 pixels. Subsequent analysis discussed in § 5.3 confirmed this data. Our absolute positions assume that the central star in our field (WFPC2 4-454) has the position stated in the published catalog (Williams et al. 1996).

5. DATA REDUCTION

Data reduction procedures utilized the Interactive Data Language (IDL) software environment for most of the basic data analysis. KFOCAS (K. Adelberger & C. C. Steidel 1996, private communication to STScI), a derivative of FOCAS (Jarvis & Tyson 1981; Valdes 1982) provided the source detections listed in the catalog. In order to provide a cross-check on the images and catalog presented in this paper, we have deliberately reduced and analyzed the data in two separate and independent ways. Specifically, in addition to the IDL and KFOCAS procedures, we utilized an independent IRAF-based image processing algorithm and an alternative source extraction program, SExtractor (Bertin & Arnouts 1996). The IDL and KFOCAS reduction procedures are described in detail as they produced the bulk of the information on the sources listed in the catalog. Descriptions of the IRAF and SExtractor reductions are provided when they differ substantially from the IDL and KFOCAS reductions.

5.1. IDL Image Reduction

Each 896 s SPARS64 integration produced an individual image. A set of 55 SPARS64 dark integrations of the same duration as the HDF exposures provided the required dark frames for the analysis. These dark exposures occurred just prior to and coincident with the HDF exposures. The data

reduction procedures produce a completely processed image for each integration. Section 5.3 describes the combination of the images into the final mosaic.

5.1.1. Dark Frames

Dark frame reductions begin with the division of each 17 sample SPARS64 darks into 16 first differences. A first difference is simply the difference between a readout and the previous readout. The first differences are then combined via a sigma clipping mean to produce a final superframe that is free of cosmic rays to the 3 σ level of the 55 combined observations. Although for most observations a simple median of first differences would suffice, observations at the sensitivity level of the HDF required sigma clipped means to avoid digitization noise. The average Camera 3 dark current is 0.2 electrons s^{-1}. In each 64 s first difference, about 12.8 electrons accumulate. The detector gain for Camera 3 is 6.5 electrons per ADU for an average of 2 ADUs per first difference. If medians are taken of these observations, there would still be 50% noise even for an infinite number of integrations. The first differences are then recombined to produce a ramp dark for subtraction from the imaging integrations. The ramp dark is a sequence of summations ranging from just the initial first difference, the initial and second first difference, to the total of all of the first differences.

5.1.2. Image Frames

Analysis of the image integrations starts with the production of a set of 16 ramp readouts for the 17 samples from each SPARS64 integration. Subtraction of the superdark ramp from each integration produces a set of dark current–corrected but not sky-corrected integrations. A set of standard linearity corrections is next applied to pixels that have exceeded the linear signal response region but have not saturated. In practice only bad "hot" pixels receive a correction owing to the low signal levels in the HDF observations.

After correction for linearity, the integrations are corrected for cosmic rays by fitting a linear function to the ramp values. The slope of this function is the signal rate in ADU per second. Cosmic rays produce an instantaneous discontinuity in the signal function. Subtraction of the fitted function from the signal produces an output that has a distinctive S shape if a cosmic ray is present. In one readout the difference between the fit and the signal transitions from negative to positive. Detection of a transition greater than expected from noise indicates the presence of a cosmic ray. The offending first difference is then removed from the ramp, and a new fit is calculated. The new fit is again checked for cosmic rays, and detected cosmic rays are removed in a similar matter. Any fits still beyond the expected noise are declared bad and flagged as bad. If the cosmic ray produces saturation, only the readouts before saturation are used in the final fit. All detected cosmic rays are recorded in the data-quality image extension. This procedure is unique to the NICMOS instrument on *HST* owing to the ability to read out nondestructively the detector during the integration. Further cosmic-ray removal can occur if necessary during the image mosaic construction in the standard manner.

Before the flat field can be applied, all of the quadrant biases in the individual images must be removed. If there is a bias level in the image, the flat-field function will produce

variations in the bias that will remain in the data. The removal procedure can be iterative, but in practice one iteration is sufficient. The first step produces a median of all of the cosmic-ray–corrected images. This median is then subtracted from each individual image. If there are no quadrant biases, the median value in each detector quadrant should be zero since the dark current and sky are removed by the subtraction. The sources do not dominate the image, so they contribute very little to the median. The second step measures the median of each quadrant in each image and records the value. The final step then subtracts these quadrant bias levels from each cosmic-ray–corrected image. The flat-field correction was then applied to each image.

The bad pixels are marked from a bad pixel mask determined from the previous observing history with the NICMOS Camera 3. The bad pixel mask contains both low response pixels and hot pixels defined as pixels with an excessive dark current. In each image the bad pixels were replaced by the median of the total image. The drizzle mosaic process does not use pixels marked as bad in the final image construction.

The median of all of the final individual images determines the level of the sky emission. The raster and dither of the large number of images reduces the source contribution of the median to a value less than the expected noise level. Inspection of the median image did not reveal any source contributions. Subtraction of this sky level from each image completes the analysis of the individual images. The median sky level in the F160W filter is 0.55 electrons s^{-1}, which is lower than the original estimates prior to the observations. This is not surprising as one of the selection criteria for the HDF was a low zodiacal background.

5.2. IRAF Image Reduction

For comparison with the IDL procedures, images were reduced in an independent pipeline using NICRED 1.5 (McLeod 1997; Lehar et al. 1999) and modified IRAF scripts developed to reduce Camera 3 images taken in parallel mode (Yan et al. 1998). Two median sky-dark frames were produced, one from the first exposure in each orbit and one from combining the second and third exposures in each orbit, to minimize the effect of any pedestal in the first exposure. These were used as dark frames along with the same flats utilized in the IDL reductions. These flats, observed on 1997 December 23, are identical to the flats used in the IDL reduction. The residual bias levels in the individual quadrants were removed by fitting a Gaussian to a histogram of the pixels in each quadran and subtracting the peak value. A new bad pixel mask was created from the exposures. The images were inspected, and any remaining cosmic-ray hits or satellite trails were individually masked.

5.3. Mosaic Techniques

Both of the data reduction procedures utilize modified versions of the drizzle software developed for the reduction of the WFPC2 HDF images. The drizzled pixel size in each case is $\sim 0\rlap{.}''1$, one-half of the original NICMOS Camera 3 pixel size. The drizzle parameter PIXFRACT is 0.6 in the drizzling of the IDL reductions, while it was set to 0.65 in the drizzling of the IRAF results.

5.3.1. IDL Image Mosaic

The first task of mosaic production is an accurate determination of the relative offsets between the individual inte-

grations. We compared offset information from the world coordinates in the header files, shifts computed from the IRAF/STSDAS Dither package, offsets from the IRAF imcentroid package of five individual objects in the field, and finally individual inspection via interactive IDL tools. The NICMOS geometric distortions have been determined to be negligible so no geometric distortion corrections were made.

In general, the agreement among the four methods was quite good. For the F160W images the discrepancy between the world coordinate shifts and the IRAF-generated shifts fell between -0.2 and 0.4 pixels in x with a mean of 0.15 (rms = 0.03) and a range of -0.5 to 0.2 pixels in y with a mean of -0.15 (rms = 0.03). The internal difference between the shifts determined by IRAF procedures averaged -0.02 pixels.

For the F110W filter the difference between the world coordinate shifts and those determined by IRAF procedures varied from -2.0 to 0.7 pixels in x and -0.4 and 2.7 pixels in y with means of 0.1 (rms = 0.14) and 0.7 (rms = 0.36), respectively. The mean internal difference between the IRAF procedures was -0.12 for x and 0.04 in y. The large excursions of 2.0 and 2.7 pixels in x and y were seen in only two images. The IRAF Dither and imcentroid positions agreed to 0.1 pixels in these images. Visual inspection of the images confirmed the IRAF positions. In both the F160W and the F110W filters the rotation angle varied by less than $0\rlap{.}°005$ owing to the excellent effort of the MOSES group in limiting the roll during the single guide star observations.

The data were drizzled using Drizzle Version 1.2 February, 1998 (Fruchter & Hook 1997) with image offsets derived from the mean of the IRAF procedures since in cases in which the IRAF positions differed from the world coordinates, interactive inspection via the IDL tools confirmed the IRAF positions. As discussed above, no geometric distortion correction or image rotation was required. High cosmic-ray persistence noise levels after transit of the South Atlantic Anomaly (SAA) required removal of 28 F160W integrations and 36 F110W integrations from the final mosaic image. A comparison of a straight combination of the drizzled frames and a combination averaged with 3 σ clipping showed no differences, which indicates that the IDL cosmic-ray removal techniques were effective.

5.3.2. IRAF Image Mosaic

The IRAF reduction images were drizzled (Drizzle Version 1.1; Fruchter et al. 1997) with offsets determined from the centroid of the central star (NICMOS 249) in each frame. No rotation or geometric distortion corrections were necessary. Owing to persistence of cosmic rays encountered in SAA passages, 25 F160W images and 37 F110W images were removed from the final mosaic. Which frames to remove was determined independently by inspection, which leads to the slight difference from the number not included in the IDL image mosaic. The drizzled frames were averaged with 3 σ clipping to remove any residual low-level cosmic rays.

6. THE IMAGES

Figures 2 and 3 show the F110W and F160W images, respectively, produced by the IDL image reduction and drizzle procedures described in the preceding section. The raster pattern of observations produces much lower signal-to-noise ratio areas in the image at the edges at which the
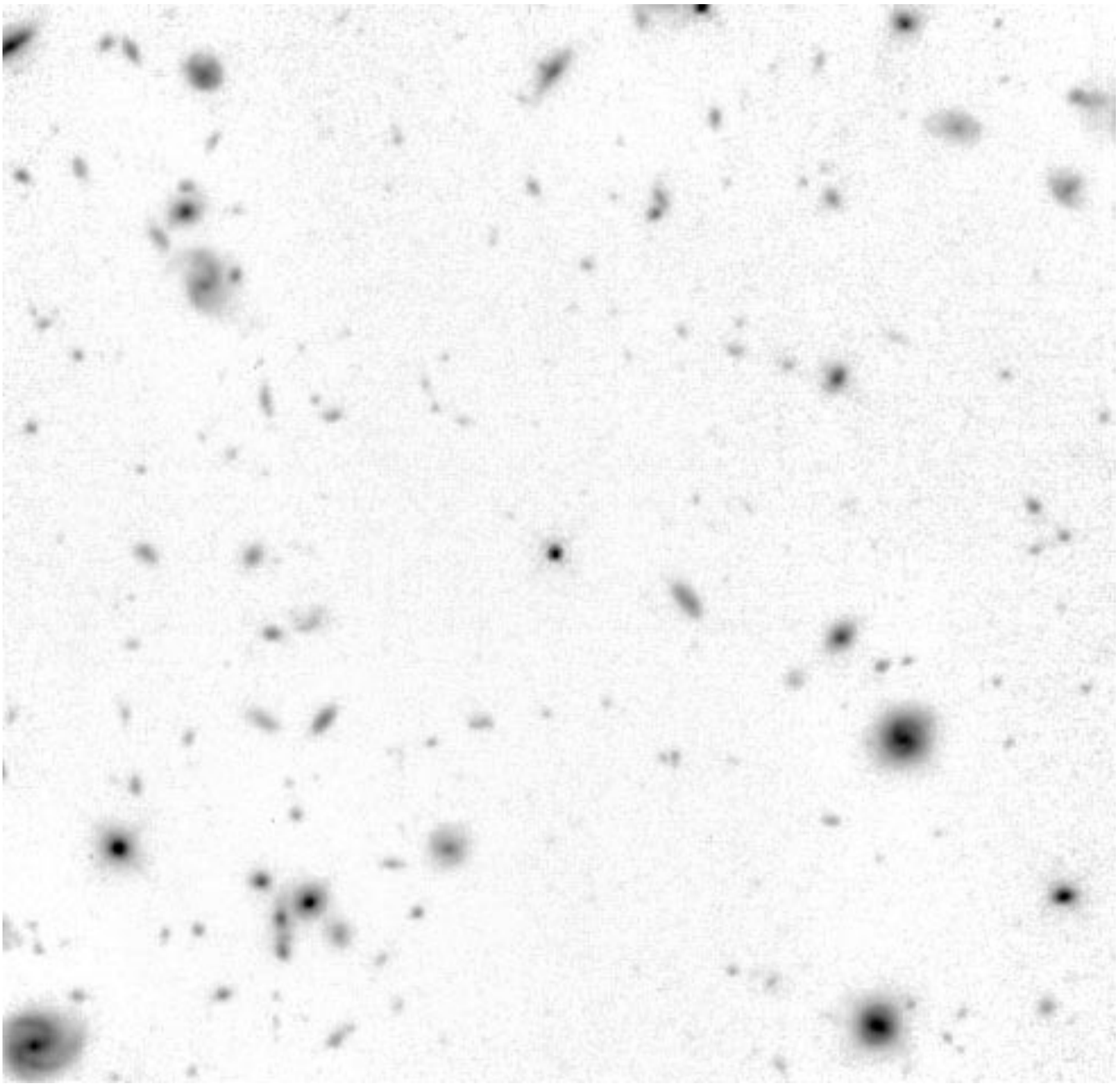
Fig. 2.—F160W image

number of overlapping integrations are greatly reduced. These areas are deleted from the image even though many strong sources are evident in these regions. The area covered by the images is a $49\overset{''}{.}19 \times 48\overset{''}{.}53$ (481×476 pixels) rectangle. Figure 4 is a color composite of the two infrared images and the F606W WFPC2 image. The WFPC2 image has been rotated and resampled to fit the orientation and pixel size of the NICMOS images. The red, green, and blue colors represent the F160W, F110W, and F606W intensities. As with the original WFPC2 color image, the stretch and color curves have been manipulated to show faint objects while preserving the detail of features in the brighter objects. This image should not be used for quantitative purposes. Figures 2 and 3 are also stretched to show the best range of features. The very high dynamic range of the image can not be displayed in a linear intensity image.

7. SOURCE DETECTION AND PHOTOMETRY

Since the original WFPC2 HDF catalog (Williams et al. 1996) utilized KFOCAS to generate its listings, our primary catalog listings also utilize KFOCAS to provide consistency. We also provide a description of the SExtractor source extraction process. The main difference between KFOCAS and FOCAS is the utilization of a supplemental image by KFOCAS that specifies the relative detectivity at each point in the image. This is important for the NICMOS HDF images where there are significant variations of quantum efficiency and total integration time over the image area.

7.1. Estimation of the Input Sigma for KFOCAS

KFOCAS uses a constant 1 σ level that is either deter-
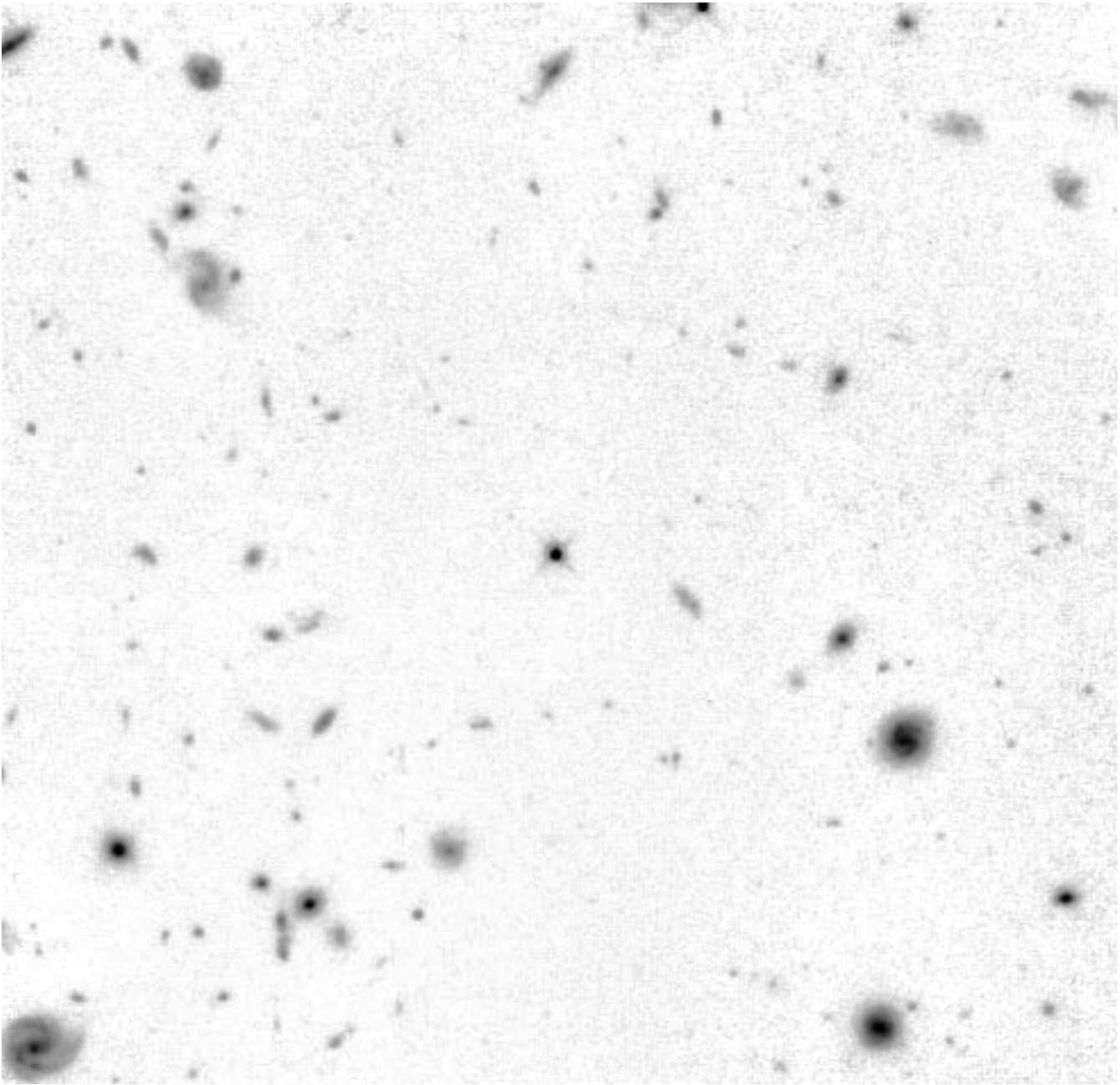
Fig. 3.—F110W image

mined from the first few lines of the image or is input manu-
ally by the user. Since the first few lines of the NICMOS
image have much lower signal-to-noise ratio than rest of the
image, we estimated the 1 σ value manually from a histo-
gram of the signal levels in all of the pixels. Figure 5 gives
the histogram of the pixel values in the two dithered images
shown in Figures 2 and 3. Only the pixels from the area
covered by the images are used in this histogram. The histo-
gram peaks at zero signal as expected for sky-subtracted
observations. The long extensions of the histograms toward
positive values owing to the sources in the field are cut off in
this figure. The flat-fielding process multiplies the true noise
value in the image by the value of the flat field. This process
raises the noise level in low quantum efficiency areas and
lowers it in high-efficiency areas. Since the median efficiency

of the area is set to 1, this process should not appreciably
alter the width of the curve.

As learned in the production of the WFPC2 images, the
drizzling process produces a correlated image and hence
correlated noise (Williams et al. 1996; A. Fruchter 1998,
private communication). There is approximately a factor of
2 reduction in the apparent noise as a result of the drizzle
process for a factor of 2 reduction in linear pixel size. The
numbers given in Figure 5 should therefore be multiplied by
a factor of 2 to determine the true 1 σ value of the noise.
This gives the noise figures of 1.22×10^{-9} Jy for the F160W
filter and 1.54×10^{-9} Jy for the F110W filter. These are the
powers that produce a signal equal to a 1 σ noise in a single
pixel. Use of these levels resulted in KFOCAS missing a
large number of real sources easily identified by eye. We
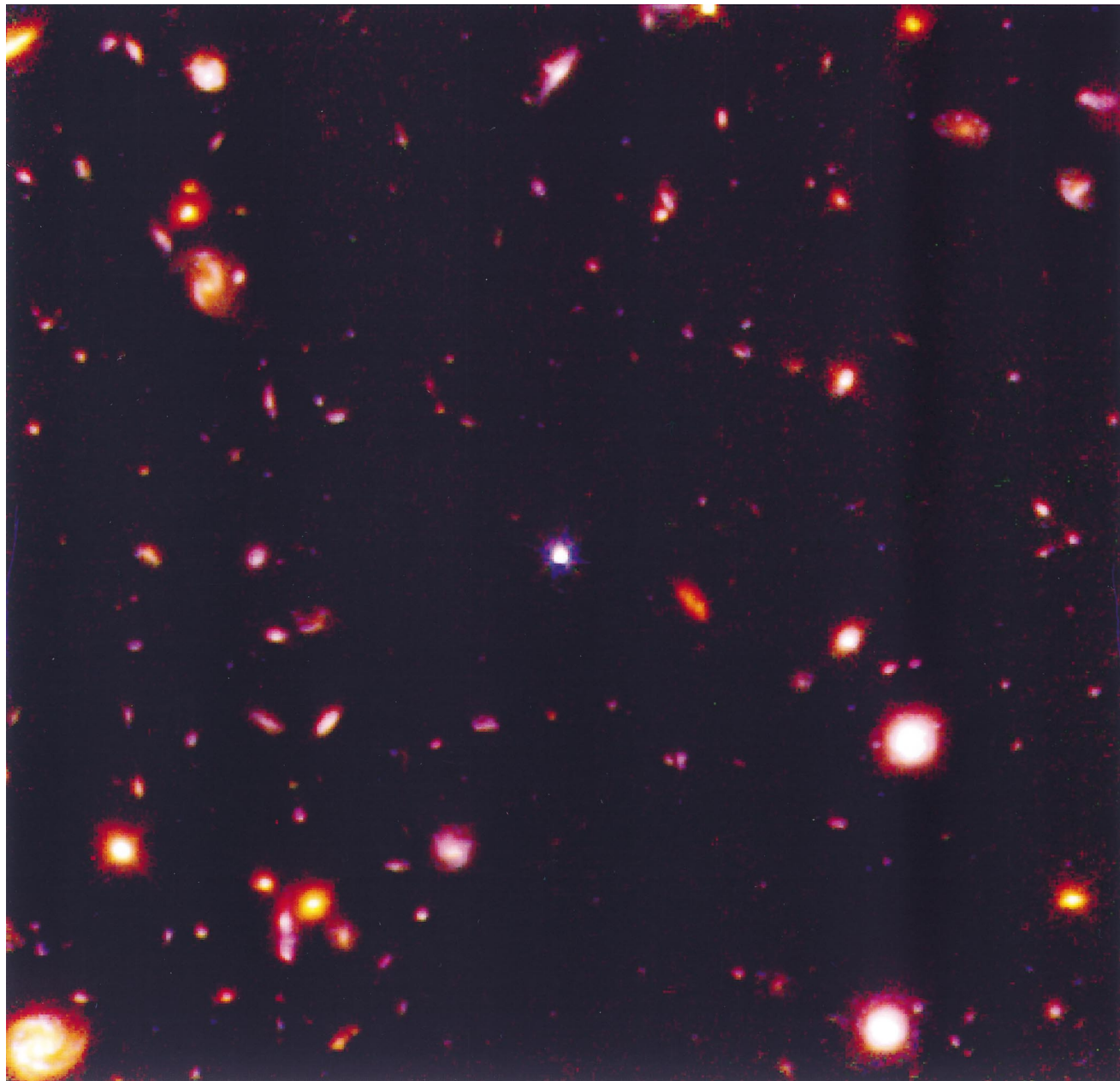
Fig. 4.—Composite color image

therefore dropped the 1 σ estimates to a very low value of 5.5×10^{-10} Jy or 2.0×10^{-4} ADUs s^{-1} for the F160W filter and 3.5×10^{-10} Jy or 2.3×10^{-4} ADUs s^{-1} for the F110W filter. The number of σ for the detection limit was then varied until all known real sources were detected without excessive over selection. It is of course the product of the chosen 1 σ noise level and the number of sigma for detection parameter that determines the signal value a pixel must have to be considered a potential source. A known real source is an object easily seen by eye in the NICMOS images that is exactly coincident with an observed source in the WFPC2 HDF images. A more rigorous discussion of the completeness and reliability of the selected sources occurs in §§ 9 and 10. The catalog listings are limited to sources with signal-to-noise ratios that exceed or equal 2.5. This discards some sources that by many tests appear to be real but eliminates a large number of sources that have a significant chance of being false.

7.2. KFOCAS Reduction

We prepared the drizzled images for the KFOCAS procedure by multiplying the signal in ADUs s^{-1} by 10^5 and subtracting the minimum value, a negative number, from the multiplied image. This produced an image that had no negative values and in which all of the significant values were well represented in the integer arithmetic used by KFOCAS. The zero-point magnitudes of the modified images are 35.3 for the F160W image and 35.186 for the F110W image. The source extraction utilized the standard KFOCAS procedures of the series KDETECT, KSKY, KEVALUATE, KSPLIT, and RESOLUTION. Our drizzled pixels have 6.25 times the area of the WFPC2 drizzled pixels; therefore, we set the minimum area for detection in pixels to 2 in order to avoid missing very compact galaxies. The parameters for the KFOCAS reduction are listed in Table 2. The point-spread function (PSF) matrix for
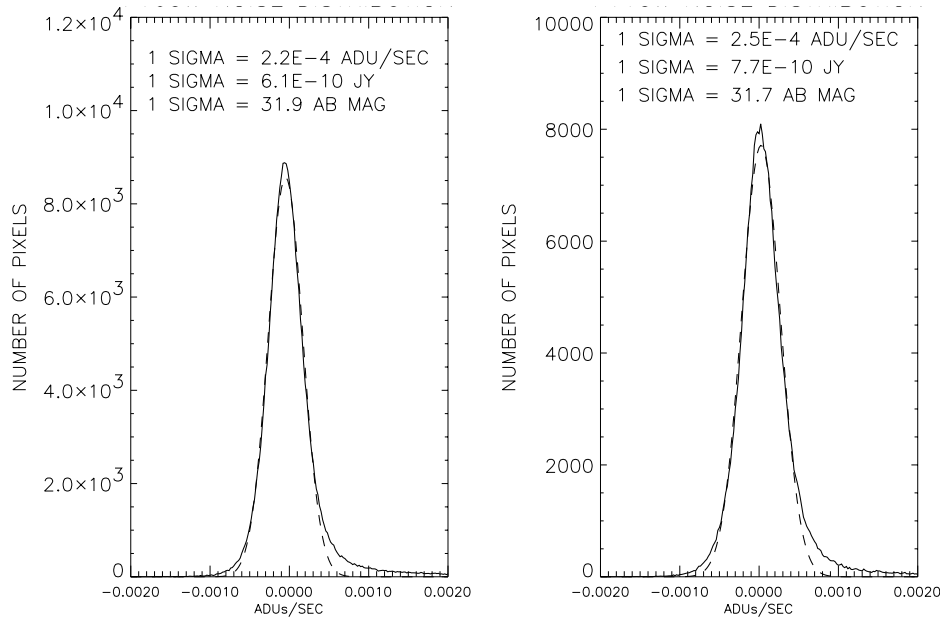
FIG. 5.—Histograms of the pixel values in the F160W (*left*) and F110W (*right*) mosaic frames are shown. Gaussian fits are overplotted as dotted lines. The measured 1 σ noise levels per pixel are 2.2×10^{-4} ADUs s^{-1} (6.1×10^{-10} Jy, 31.9 AB mag) for the F160W image and 2.5×10^{-4} ADUs s^{-1} (7.7×10^{-10} Jy, 31.7 AB mag) for the F110W image. The true noise levels are about a factor of 2 higher than these values owing to the correlated noise produced in the drizzling process.

smoothing the data is a 3×3 matrix that mimics the PSF of the central star in the drizzled data. This is much more sharply peaked than the Gaussian function used in the SExtractor analysis.

7.2.1. *Preparation of the Detectivity Image*

Each pixel, pix$_{i,j}$, in the final image has a quality $Q_{i,j}$ value associated with it. The quality value is the square root of the sum of the squares of the total efficiency of each pixel in the individual image that contributes to the final image. Owing to the raster and dither pattern, a pixel in the final image has contributions from many different individual image pixels.

$$Q_{i,j} = \sqrt{\sum_{k=1}^{n} (\text{eff}_k)^2} \ . \tag{1}$$

Here n is the number of pixels contributing to the final image pixel, pix$_{i,j}$, and the efficiency eff$_k$ of each contributing pixel is measured by the inverse of its multiplicative flat-field value. Figures 6 and 7 show the detectivity functions over the image areas used in the catalog.

7.3. *SExtractor Reduction*

As a cross-check on the KFOCAS detections we utilized an alternative source extraction system, SExtractor, on data

TABLE 2

KFOCAS PARAMETERS

KFOCAS Parameter	F160W	F110W
Magnitude zero point	35.3	35.186
Catalog magnitude limit	100.	100.
Radius of fixed circular aperture	6.0	6.0
Sigma of sky	20	22
Sigma above sky for detection.................	2.5	3.0
Sigma below sky for detection.................	20.0	20.0
Minimum area for detection	2	2
Significance for evaluation and splitting......	0.15	0.15

reduced via the IRAF reduction procedure rather than the IDL based procedure.

7.3.1. *Galaxy Detection*

We performed object detection on the F160W images and photometry on the F160W and F110W images using SExtractor version 2.0.7 (Bertin & Arnouts 1996). The final F160W and F110W images reduced in the IRAF pipeline showed low-frequency structure in the background in the
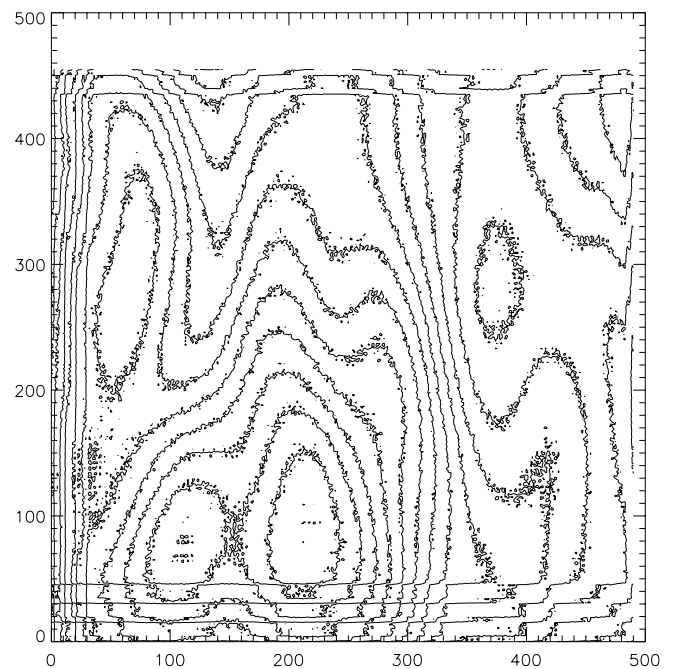
FIG. 6.—F160W source detectability contours for the region included in the catalog. The contours inside the F160W area cover a factor of 3.77. The contour levels are 5% of this range. The regions with the highest detectivity are in the center and lower left.

Fig. 7.—F110W source detectability contours for the region included in the catalog. The contours inside the F110W area cover a factor 4.75. The contour levels are 5% of this range. The regions with the highest detectivity are in the center and lower left.

TABLE 3
SExtractor Parameters

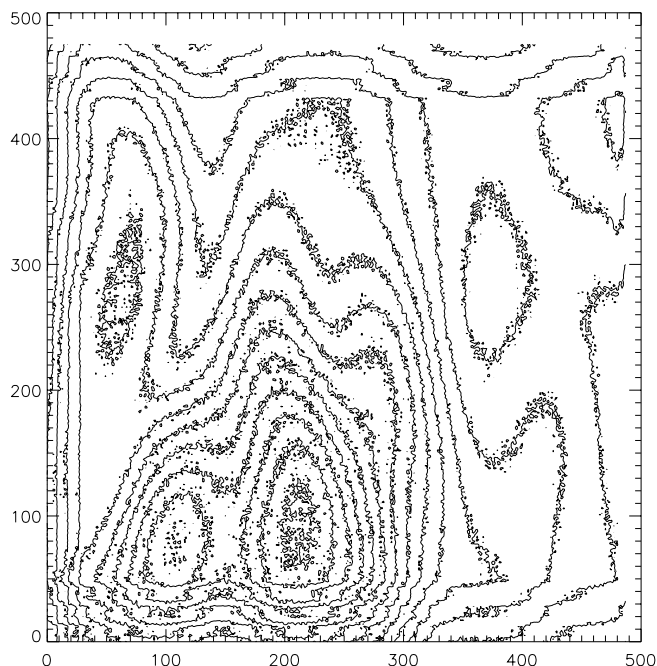| Parameter	Value
DETECT_MINAREA	2
DETECT_THRESH	2.15
ANALYSIS_THRESH	2.15
FILTER_NAME	gauss_2.0_3x3.conv
CLEAN	N
MASK_TYPE	CORRECT
WEIGHT_TYPE	MAP_WEIGHT
PHOT_APERTURES	6
GAIN	6.5
PIXEL_SCALE	0.1
SEEING_FWHM	0.2
BACK_SIZE	64
BACK_FILTERSIZE	3
BACKPHOTO_TYPE	LOCAL
BACKPHOTO_THICK	24
MAG_ZEROPOINT	22.80 (F160W)
MAG_ZEROPOINT	22.68 (F110W)

X-direction. We created background frames in SExtractor using a 64×32 mesh, which were subtracted from the reduced frames, producing cosmetically more uniform backgrounds. We measure 1 σ noise levels from histograms of all the pixels in the frames of 2.0×10^{-4} ADUs s^{-1} in the F160W image and 2.4×10^{-4} ADUs s^{-1} in the F110W frame, consistent with the values shown in Figure 5. The amplitude of the fluctuations in the background varies by up to 50% across the image owing to variations in the quantum efficiency of the detector and the dither pattern used. Thus we used the option in SExtractor (WEIGHT_TYPE) that accepts a user-supplied variance map (for which we used the "detectivity" function described in § 7.2.1). SExtractor robustly scales the weight map to the appropriate absolute level by comparing the weight map to an internal, low-resolution, absolute variance map built from the science image itself. In contrast to the KFOCAS source extraction, all object detection was done on the F160W image, and magnitudes were measured to the corresponding isophotes on the F110W image.

After experimenting with different values of SExtractor parameters, we adopted the values given in Table 3. Aside from the determination of the local variance itself, the three most critical parameters that affect the detection of very faint isolated sources are FILTER_NAME, DETECT_MINAREA, and DETECT_THRESH. The FILTER_NAME parameter describes the smoothing kernel that is applied to the image, and for this a Gaussian with a full width half-maximum of 2.0 (drizzled) pixels was used over a 3×3 pixel grid. We tested various combinations of DETECT_MINAREA, the minimum number of contiguous pixels above a level that is the product of the parameter DETECT_THRESH times the local rms fluctuation in the background. Our final choices for these parameters are DETECT_MINAREA = 2 pixels

and DETECT_THRESH = 2.15 σ. This choice for DETECT_MINAREA (the same value as for the equivalent KFOCAS parameter) favors slightly the detection of the most compact sources, and the final choice of 2.15 for DETECT_THRESH was dictated by an attempt to strike a judicious balance between completeness and reliability. We tested an alternative set of parameters with DETECT_MINAREA set to 3 pixels and with DETECT_THRESH to a lower value in order to detect the same number of sources as with DETECT_MINAREA = 2 and DETECT_THRESH = 2.15. Estimating the number of false detection rates and completeness as discussed in §§ 9 and 10, we found that these two sets of parameters behaved very similarly. For the reason stated above, we selected DETECT_MINAREA = 2. Sections 9 and 10 contain a more quantitative discussion of the completeness and reliability of the detected sources.

Although as with the KFOCAS reductions we have deliberately erred on the side of extracting a fairly large estimated fraction of false detections (at the faintest levels) and a completeness level that is only of order 50%, the catalog listings contain only sources with signal-to-noise ratios greater than 2.5.

7.4. Comparison of the IDL-KFOCAS and the IRAF-SExtractor Photometry

At this point our analysis contains four components, the IDL and IRAF reduced images and the KFOCAS and SExtractor source extractions and photometry. In the spirit of independent cross-checks, it is useful to compare these results and to see if any differences lie primarily in the images or in the source extraction procedures. We will discuss the differences in completeness and reliability between the two methods after §§ 9 and 10. Data presented so far have been for either the IDL-KFOCAS or IRAF-SExtractor procedures. The third panel in Figure 8 shows a comparison between the aperture magnitudes found by KFOCAS in the IDL image and the aperture magnitudes found by SExtractor in the IRAF images for all objects detected in common. The delta magnitudes are KFOCAS magnitude minus SExtractor magnitude. In both cases the diameter of the aperture is 0″.6.
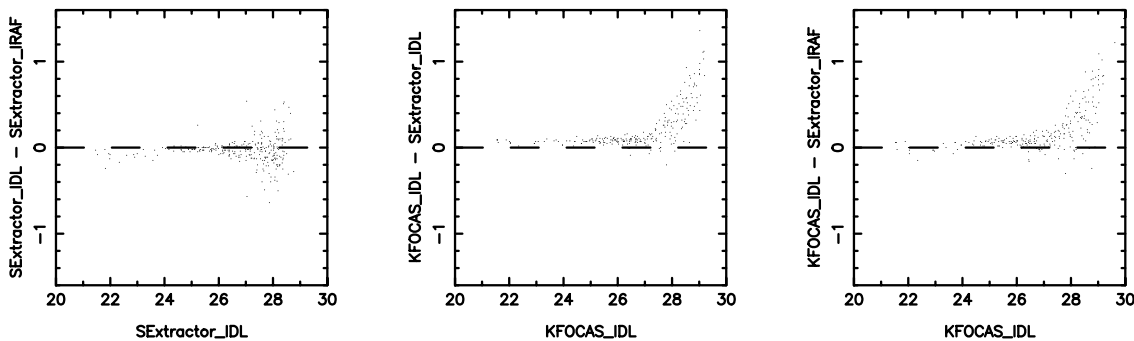
Fig. 8.—Comparison of KFOCAS and SExtractor aperture magnitudes before the catalog cut at 2.4 σ. The first panel shows the difference in SExtractor magnitudes determined from the IDL and IRAF images. The second and third panels indicate the differences between the two source extraction programs, KFOCAS and SExtractor. The last panel is a good guide in comparing the SExtractor determined magnitudes in the catalog with those determined by KFOCAS

As expected, the correlation is very good at bright magnitudes and gets worse at the faint end. The SExtractor magnitudes are equal to the KFOCAS magnitudes up until 28th magnitude, where the SExtractor magnitudes become significantly brighter than the KFOCAS magnitudes. These differences could be due to differences either in the input images or in the magnitudes extracted by KFOCAS and SExtractor. To check this, we ran SExtractor on both the IDL-reduced and the IRAF-reduced images. The first panel in Figure 8 shows the result of this test, which shows a uniform scatter about the zero level at the fainter magnitudes. The slight offset at the bright end is probably due to the IRAF procedure IMCOMBINE clipping some pixels in the brightest galaxies in the IRAF image. A follow-up test comparing the KFOCAS reductions of the IDL image with SExtractor reductions of the IDL images is shown in the middle panel of Figure 8. This plot is essentially identical to the last panel except for about a 0.07 mag offset at the brighter end. This set of tests shows that the differences between the KFOCAS/IDL magnitudes and the SExtractor/IRAF magnitudes shown in the last panel of Figure 8 are entirely due to the differences between the KFOCAS and SExtractor algorithms, not from any differences between the IDL and IRAF image production procedures. The origin of this difference is not clear, but the reader should be aware that these two standard procedures do produce differences at the very faintest levels.

8. THE CATALOG

Table 4 contains the catalog of sources from the KFOCAS source extraction from the F160W and F110W images. This catalog contains only sources with signal-to-noise ratios greater than 2.5. We anticipate a future publication describing the sources with less reliable detections. The catalog contains 342 objects, some of which are components of a larger object. The catalog contains 235 objects in common with the WFPC2 catalog. Two-hundred twenty-one objects have detections in both filters, 56 objects have a detection only in the F160W filter, 53 have a detection only in the F110W filter, and none have detections only in SExtractor. The objects are arranged by right ascension, which sometimes separates different components of the same object in the catalog. The data and numbering in the catalog have the priorities, in order, of F160W KFOCAS, F110W KFOCAS, and SExtractor. This means that all

KFOCAS objects detected in both filters use the KFOCAS F160W R.A., decl., and x and y positions. The magnitudes come from the KFOCAS F160W and F110W extractions. Positional coincidence is relative to the F160W positions. Objects that have F110W KFOCAS detections but not KFOCAS F160W detections use the F110W KFOCAS positions and magnitudes. The catalog columns contain the following parameters.

ID.—This is a running number for each object. The numbers after the decimal point indicate the level of splitting by KFOCAS up to three levels of daughter objects. Since the list is arranged by right ascension, daughter objects can appear separately from the parent objects. No object is repeated. Numbers of 900 or higher are split F110W objects that are not coincident with any F160W split even though some of the components are in common.

WFPC.—The WFPC column lists the nearest WFPC2 source from the Williams et al. (1996) catalog. This is not necessarily the same object, just the nearest.

s.—The s-value is the separation in arcseconds between the NICMOS and the nearest WFPC2 object as listed in the WFPC column. A large value of separation indicates that the NICMOS and WFPC2 object are probably not associated.

x and y.—These columns give the x- and y-values of the centroid of the source in the F160W or F110W image. If the object is detected in both images, the x- and y-values refer to the F160W image. Objects detected only by SExtractor have the values determined by SExtractor. This order of precedence holds for all of the subsequent values.

R.A. and Decl.—These columns give the right ascension and declination of the centroid of the source. Only the minutes and seconds are listed. The hour of right ascension is 12^h for all sources, and all sources have $62°$ of declination. The source positions assume that the central star, NICMOS 145, and the WFPC2 object 4-454 have the same position and that the measured plate scales of the NICMOS Camera 3 are correct. In this sense all positions are relative to the position of the WFPC2 4-454 object.

$t_{160}, i_{160}, a_{160}, t_{110}, i_{110},$ *and* $a_{110}.$—These are the total, isophotal, and aperture magnitudes found by KFOCAS in the F160W and F110W images. The aperture diameter for the aperture magnitudes is $0\overset{''}{.}6$. The total and isophotal magnitudes are as described in Williams et al. (1996). A value of 99.99 indicates that the object was not detected in

TABLE 4

CATALOG OF DETECTED SOURCES

ID	WFPC	s (arcsec)	x	y	R.A.	Decl.	t_{160}	i_{160}	a_{160}	t_{110}	i_{110}	a_{110}	S/N	A (arcsec^2)	r_1 (arcsec)	Tests
1.0000	4-851.0	0.31	560.40	134.80	36 40.81	12 09.258	28.56	28.86	28.54	28.85	29.17	28.47	2.553	0.180	0.163	20100
2.0000	4-830.0	0.10	561.00	152.00	36 40.95	12 10.67	27.43	27.76	27.42	27.87	28.21	27.92	6.434	0.220	0.122	21111
3.0000	4-810.0	0.08	579.80	180.00	36 40.98	12 14.13	28.18	28.78	28.08	99.99	99.99	99.99	3.502	0.190	0.084	10010
4.0000	4-851.0	2.45	540.50	127.00	36 40.98	12 07.445	99.99	99.99	99.99	28.86	29.28	28.63	2.804	1.142	0.050	00000
5.0000	4-822.0	0.08	550.08	158.03	36 41.13	12 10.50	24.50	24.65	25.33	24.88	25.04	25.44	22.66	2.360	0.277	22111
6.0000	4-813.2	1.48	526.50	135.00	36 41.22	12 07.239	99.99	99.99	99.99	28.80	29.46	28.41	2.974	0.968	0.043	01000
7.0000	4-766.0	0.91	574.50	201.00	36 41.29	12 15.56	99.99	99.99	99.99	28.89	29.42	28.56	2.746	1.010	0.062	00000
8.0000	4-766.0	0.88	566.25	197.75	36 41.29	12 14.73	28.69	29.36	28.34	99.99	99.99	99.99	2.570	0.140	0.072	10000
9.0000	4-766.0	0.47	568.66	210.66	36 41.37	12 15.94	28.69	29.68	28.48	99.99	99.99	99.99	2.861	0.110	0.085	00000
10.0000	4-813.2	0.21	514.50	141.00	36 41.40	12 06.992	99.99	99.99	99.99	28.94	29.23	28.55	2.605	1.200	0.046	01010
11.0000	4-790.0	0.21	539.33	175.66	36 41.41	12 11.30	28.73	29.36	28.52	27.73	28.16	27.82	2.857	0.110	0.069	22111
12.0000	4-813.2	0.15	511.72	139.27	36 41.41	12 06.649	27.18	27.44	27.16	27.26	28.15	27.13	7.199	0.270	0.109	21111
13.0000	4-767.0	1.05	551.75	198.00	36 41.47	12 13.92	99.99	99.99	99.99	28.46	28.97	28.15	2.640	0.760	0.102	01000
14.0000	4-767.0	0.08	557.46	207.10	36 41.47	12 14.97	21.53	21.56	22.04	22.10	22.13	22.55	157.7	7.990	0.267	22111
15.0000	4-813.0	0.08	506.15	144.57	36 41.53	12 06.731	25.94	26.14	26.18	26.37	26.61	26.48	12.36	0.750	0.162	21111
16.0000	4-794.0	0.02	512.73	155.56	36 41.55	12 08.022	25.98	26.29	26.43	26.39	26.85	26.67	11.24	0.830	0.190	22111
17.0000	4-739.0	0.75	562.00	227.00	36 41.59	12 16.86	28.35	29.10	28.31	99.99	99.99	99.99	4.062	0.110	0.054	10000
18.0000	4-760.0	0.35	537.44	194.77	36 41.60	12 12.71	27.73	28.19	27.83	29.17	29.78	28.87	4.568	0.250	0.132	22101
19.0000	4-802.0	0.65	493.00	135.50	36 41.61	12 05.221	99.99	99.99	99.99	28.68	29.56	28.51	2.843	0.887	0.062	00000
20.0000	4-802.0	0.06	488.50	130.62	36 41.61	12 04.507	26.46	26.97	27.17	27.34	27.73	27.40	7.592	0.740	0.204	21110
21.0000	4-739.0	0.06	555.60	223.00	36 41.63	12 16.13	28.08	28.75	27.99	99.99	99.99	99.99	4.206	0.160	0.093	20011
22.0000	4-802.0	0.98	491.50	140.50	36 41.66	12 05.495	28.46	28.97	28.35	99.99	99.99	99.99	3.402	0.120	0.082	10000
23.0000	4-706.0	1.15	569.00	249.50	36 41.71	12 19.16	99.99	99.99	99.99	28.78	29.37	28.57	2.582	1.054	0.040	01000
24.0000	4-706.0	1.06	567.50	248.00	36 41.72	12 18.94	99.99	99.99	99.99	28.86	29.59	28.39	2.817	0.862	0.056	01000
25.0000	4-683.0	0.97	572.75	270.25	36 41.84	12 21.04	28.55	28.99	28.58	99.99	99.99	99.99	2.750	0.160	0.078	10000
26.1200	4-795.112	0.09	489.40	159.18	36 41.85	12 06.910	25.70	25.78	25.72	25.68	25.74	25.75	18.94	0.680	0.160	22111
26.1000	4-795.0	0.13	476.22	150.64	36 41.93	12 05.303	20.16	20.21	21.55	20.52	20.58	21.90	336.0	17.63	0.510	22111
26.0000	4-795.0	0.12	474.67	150.20	36 41.93	12 05.303	20.16	20.19	21.55	20.52	20.58	21.90	272.2	22.53	0.534	22111
26.1100	4-795.0	0.13	475.39	150.33	36 41.93	12 05.289	20.17	20.24	21.55	20.52	20.58	21.90	474.9	11.49	0.475	22111
27.0000	4-665.0	0.04	567.34	298.55	36 42.16	12 23.01	25.83	26.04	26.16	25.90	26.19	26.26	13.39	0.790	0.170	21111
28.0000	4-652.0	0.04	575.60	314.80	36 42.20	12 24.84	28.47	28.87	28.43	28.72	29.30	28.16	2.765	0.180	0.085	22210
26.2000	4-757.0	1.14	454.33	154.00	36 42.21	12 04.328	27.61	27.66	26.93	26.60	26.93	27.01	5.781	0.230	0.110	11101
29.0000	4-769.0	0.18	432.56	132.29	36 42.28	12 01.238	25.47	25.74	26.24	25.82	26.09	26.34	14.40	1.200	0.248	22111
30.0000	4-671.2	0.68	537.84	279.55	36 42.32	12 19.65	27.88	29.57	28.25	99.00	99.00	99.00	5.800	0.040	0.000	00003
31.0000	4-671.0	0.05	533.48	274.67	36 42.35	12 18.99	26.25	26.33	26.53	26.33	26.54	26.51	8.648	0.850	0.186	22111
32.0000	4-690.0	0.11	502.42	234.66	36 42.36	12 13.83	26.62	27.08	27.03	26.86	27.18	26.93	6.986	0.690	0.161	22111
33.0000	4-743.0	0.19	421.25	138.25	36 42.47	12 01.018	28.32	29.00	28.16	29.34	29.73	29.46	3.790	0.130	0.082	20011
34.0000	4-715.0	0.10	443.50	176.50	36 42.54	12 05.537	99.99	99.99	99.99	28.16	28.79	28.04	3.694	0.900	0.082	02011
35.0000	4-687.0	0.07	476.28	223.50	36 42.57	12 11.33	27.11	27.42	27.25	28.20	28.85	28.06	7.124	0.310	0.135	22111
36.0000	4-619.0	0.14	556.62	333.87	36 42.59	12 25.24	26.93	27.31	27.12	29.89	29.85	30.79	7.998	0.340	0.148	21111
37.0000	4-725.0	0.15	428.95	168.74	36 42.64	12 03.985	25.54	25.74	26.26	25.98	26.46	26.70	12.38	1.360	0.245	22111
38.0000	4-636.0	0.04	528.16	301.66	36 42.64	12 20.86	26.22	26.44	26.49	26.34	26.56	26.52	10.11	0.680	0.154	22111
39.0000	4-671.2	2.40	509.33	280.26	36 42.66	12 17.96	28.27	30.24	28.64	27.87	30.47	28.33	5.700	0.030	0.000	01003
40.0000	4-636.0	0.74	522.00	297.50	36 42.68	12 20.14	29.04	29.92	28.97	99.99	99.99	99.99	2.540	0.080	0.050	10001
41.0000	4-636.0	0.62	521.66	300.33	36 42.70	12 20.36	28.77	29.42	28.67	99.99	99.99	99.99	3.044	0.090	0.088	20001
42.0000	4-716.0	1.31	405.50	149.00	36 42.75	12 00.977	99.99	99.99	99.99	28.93	29.63	28.84	2.631	0.827	0.047	01000
43.0000	4-707.0	0.19	421.54	173.00	36 42.76	12 03.861	27.70	28.15	27.80	27.55	28.08	27.59	4.439	0.270	0.128	22111

TABLE 4—Continued

ID	WFPC	s (arcsec)	x	y	R.A.	Decl.	t_{160}	i_{160}	a_{160}	t_{110}	i_{110}	a_{110}	S/N	A (arcsec²)	r_1 (arcsec)	Tests
44.0000	4-561.0	1.27	578.00	393.00	36 42.86	12 31.36	28.24	28.65	28.52	99.99	99.99	99.99	3.551	0.170	0.130	20000
47.1000	4-581.0	0.03	556.85	365.35	36 42.86	12 27.86	24.93	25.09	25.36	25.48	25.63	25.67	23.10	1.370	0.212	22111
45.0000	4-716.0	0.17	392.66	145.50	36 42.86	11 59.86	28.51	29.11	28.63	28.41	28.96	28.22	2.752	0.170	0.116	20111
46.0000	4-697.0	0.08	411.57	174.40	36 42.89	12 03.353	25.81	25.94	26.12	26.66	26.87	26.74	12.80	0.860	0.177	22111
47.0000	4-581.12	0.21	551.59	363.05	36 42.89	12 27.42	24.45	24.56	25.36	28.69	29.17	28.54	20.69	2.990	0.658	11110
48.0000	4-606.0	0.06	525.50	328.00	36 42.90	12 22.85	28.50	29.23	28.35	99.99	99.99	99.99	3.221	0.130	0.088	20011
49.0000	4-656.0	0.05	486.95	276.44	36 42.90	12 16.31	20.06	20.08	21.89	20.34	20.36	22.20	299.5	22.09	0.618	22111
50.0000	4-614.2	1.59	508.01	306.80	36 42.91	12 20.03	28.06	28.74	28.43	27.99	29.59	28.45	3.300	0.090	0.000	10003
47.2000	4-581.2	0.11	545.75	360.37	36 42.95	12 26.67	25.55	25.71	25.98	25.96	26.01	26.18	15.73	1.030	0.202	22111
51.0000	4-660.0	0.17	454.80	240.43	36 42.96	12 11.38	25.27	25.37	25.79	25.92	26.13	26.29	17.34	1.190	0.225	22111
52.0000	4-554.2	0.07	545.00	370.50	36 43.05	12 27.55	99.99	99.99	99.99	28.08	28.52	27.95	3.360	0.766	0.087	01011
53.0000	4-537.0	0.33	563.50	398.00	36 43.08	12 30.91	99.99	99.99	99.99	28.60	29.18	28.12	3.585	1.253	0.045	01000
54.0000	4-664.0	0.11	422.28	213.00	36 43.10	12 07.171	28.11	28.43	27.98	28.26	28.76	28.14	3.844	0.180	0.086	22111
55.0000	4-531.0	0.09	575.60	418.36	36 43.10	12 33.26	25.68	25.88	26.10	26.02	26.29	26.43	13.33	1.000	0.192	22110
56.0000	4-537.0	0.12	562.71	401.42	36 43.10	12 31.10	28.52	28.63	28.47	99.99	99.99	99.99	2.726	0.170	0.108	20011
57.0000	4-554.0	0.03	544.77	377.70	36 43.12	12 28.12	24.32	24.38	24.80	24.39	24.56	24.84	26.95	2.370	0.247	21111
58.0000	4-695.0	0.46	381.00	166.00	36 43.18	12 00.799	28.59	28.81	28.79	99.99	99.99	99.99	2.745	0.150	0.131	10000
59.0000	4-599.0	0.04	488.50	310.70	36 43.18	12 19.17	25.76	26.00	26.03	26.66	26.81	26.67	15.02	0.710	0.154	21111
60.0000	4-541.0	0.87	534.00	371.50	36 43.19	12 26.94	99.99	99.99	99.99	28.12	28.75	28.09	3.394	0.929	0.097	00000
61.0000	4-590.0	0.09	477.28	308.59	36 43.29	12 18.30	24.85	24.90	25.20	25.27	25.42	25.62	24.57	1.250	0.206	22111
62.0000	4-531.0	1.49	565.50	429.00	36 43.32	12 33.56	99.99	99.99	99.99	28.90	29.54	28.62	2.718	0.899	0.045	00000
63.0000	4-605.0	0.12	460.80	290.90	36 43.33	12 15.86	27.62	27.99	27.57	28.33	29.11	28.23	5.433	0.220	0.109	22111
64.0000	4-677.0	0.14	368.90	175.09	36 43.40	12 00.826	27.91	28.22	27.97	99.99	99.99	99.99	3.487	0.300	0.124	20011
65.0000	4-541.0	1.26	527.81	391.54	36 43.43	12 28.21	99.99	99.99	99.99	27.28	27.75	27.47	5.091	0.852	0.175	01000
66.0000	4-541.0	1.18	525.00	389.00	36 43.45	12 27.82	99.99	99.99	99.99	28.28	28.77	28.20	3.865	1.219	0.066	00000
67.0000	4-553.0	0.01	485.66	338.33	36 43.46	12 21.26	28.86	29.29	28.48	29.15	29.34	28.84	2.822	0.090	0.086	21110
68.0000	4-565.0	0.05	459.04	321.55	36 43.62	12 18.25	22.19	22.24	23.06	22.39	22.45	23.20	106.5	5.840	0.344	22111
69.0000	4-437.0	2.44	573.66	474.66	36 43.62	12 37.74	28.74	29.30	28.78	99.99	99.99	99.99	2.837	0.110	0.054	20000
70.0000	4-669.0	0.16	330.14	155.85	36 43.68	11 56.87	28.11	28.81	28.11	28.29	28.97	28.11	3.355	0.230	0.096	20111
71.0000	4-572.0	0.04	439.20	303.01	36 43.69	12 15.50	24.82	25.01	25.88	25.05	25.26	26.01	17.41	2.310	0.308	22111
72.0000	4-598.0	0.08	411.70	266.76	36 43.69	12 10.90	27.15	27.43	27.40	27.64	28.13	27.72	5.961	0.400	0.165	21111
73.0000	4-479.0	0.60	533.66	430.66	36 43.71	12 31.75	99.99	99.99	99.99	28.52	29.21	28.82	2.767	0.814	0.073	01000
74.0000	4-513.0	0.05	493.00	381.25	36 43.75	12 25.20	28.62	29.20	28.41	29.09	29.30	28.88	2.876	0.130	0.076	21111
75.0000	4-479.0	0.04	531.88	436.91	36 43.78	12 32.11	25.85	26.04	26.20	25.98	26.12	26.14	11.83	0.940	0.170	21111
76.0000	4-525.0	0.07	473.90	362.00	36 43.80	12 22.45	27.51	27.88	27.58	27.38	27.64	27.36	5.136	0.290	0.120	22111
77.0000	4-486.0	0.07	516.00	420.00	36 43.81	12 29.74	28.66	29.46	28.54	27.86	28.46	27.91	3.030	0.110	0.062	12111
78.0000	4-513.0	0.79	486.16	384.33	36 43.86	12 25.06	99.99	99.99	99.99	27.96	28.37	28.02	3.356	0.887	0.106	01000
79.0000	4-626.0	0.13	349.00	205.75	36 43.90	12 02.103	28.41	28.91	28.36	28.28	28.83	28.20	2.858	0.190	0.111	21111
80.0000	4-444.0	0.05	545.33	480.83	36 44.00	12 36.51	27.43	27.91	27.74	28.40	29.15	28.37	5.650	0.280	0.171	22111
81.1000	4-576.0	0.18	386.20	267.80	36 44.01	12 09.450	25.37	25.98	25.91	25.58	26.01	26.06	23.56	0.670	0.171	22111
81.0000	4-576.0	0.28	384.10	267.85	36 44.02	12 09.327	25.02	25.13	25.91	25.13	25.30	26.06	18.04	1.640	0.319	22101
82.0000	4-481.0	0.13	487.50	407.00	36 44.03	12 26.96	29.23	29.81	29.00	99.99	99.99	99.99	2.504	0.060	0.050	10010
83.0000	4-500.0	0.48	464.00	376.40	36 44.04	12 23.04	28.56	29.05	28.43	28.48	29.03	28.44	2.694	0.160	0.104	11101
84.0000	4-524.0	2.69	401.00	292.50	36 44.06	12 12.40	99.99	99.99	99.99	28.68	29.15	28.72	2.833	1.294	0.075	01000
85.0000	4-494.0	1.18	473.00	389.50	36 44.06	12 24.68	99.99	99.99	99.99	28.75	29.60	28.87	2.664	0.856	0.051	01000
81.2000	4-576.2	0.06	381.50	268.00	36 44.06	12 09.148	26.40	27.01	26.44	26.31	26.74	26.51	16.23	0.250	0.114	21111
86.0000	4-500.0	0.19	462.70	380.35	36 44.09	12 23.26	26.97	27.45	27.43	27.92	28.34	27.79	7.103	0.390	0.201	22111
87.0000	4-653.0	0.19	284.09	143.00	36 44.11	11 53.01	27.78	28.17	27.85	99.99	99.99	99.99	4.064	0.280	0.115	20011
88.0000	4-430.0	0.05	559.01	519.49	36 44.18	12 40.44	22.88	22.98	24.42	23.04	23.11	24.57	50.78	6.790	0.465	21111

TABLE 4—Continued

ID	WFPC	s (arcsec)	x	y	R.A.	Decl.	t_{160}	i_{160}	a_{160}	t_{110}	i_{110}	a_{110}	S/N	A (arcsec²)	r_1 (arcsec)	Tests
89.0000	4-501.0	0.03	435.50	360.50	36 44.24	12 19.99	28.30	28.96	28.13	99.99	99.99	99.99	4.039	0.120	0.090	20011
90.0000	4-580.0	0.11	331.27	231.90	36 44.33	12 03.147	28.05	28.41	28.13	28.08	28.48	28.20	3.460	0.240	0.130	21111
91.0000	4-524.0	0.19	394.46	317.46	36 44.34	12 13.98	27.85	28.13	27.98	99.99	99.99	99.99	3.658	0.300	0.148	20011
92.0000	4-499.0	0.07	408.85	346.28	36 44.42	12 17.19	28.02	28.55	28.07	28.82	29.40	28.67	3.958	0.200	0.112	21111
93.0000	4-452.0	0.96	467.12	425.87	36 44.44	12 27.23	28.38	28.52	28.31	99.99	99.99	99.99	2.658	0.220	0.118	20001
94.0000	4-627.0	0.20	263.65	158.76	36 44.48	11 53.05	26.05	26.31	26.66	26.29	26.58	26.77	9.286	1.030	0.216	22111
95.0000	4-438.0	0.04	483.82	453.37	36 44.48	12 30.50	25.85	26.19	26.65	26.25	26.55	26.96	10.96	1.080	0.258	22111
96.0000	4-400.0	0.51	513.66	500.66	36 44.55	12 36.18	28.81	29.52	28.82	28.51	29.42	28.17	2.658	0.110	0.077	11101
97.0000	4-505.0	0.31	390.77	337.94	36 44.55	12 15.42	23.05	23.09	24.49	24.00	24.09	25.48	48.38	5.780	0.484	22101
98.0000	4-527.0	0.05	356.03	292.25	36 44.57	12 09.560	26.52	26.77	26.86	26.65	26.97	26.89	7.206	0.760	0.170	22111
99.0000	4-400.2	1.17	507.21	495.52	36 44.57	12 35.36	27.79	29.04	28.16	99.00	99.00	99.00	3.000	0.060	0.000	00003
100.000	4-472.0	0.15	418.56	378.25	36 44.59	12 20.39	27.11	27.42	27.29	28.24	28.93	27.99	6.743	0.340	0.165	22111
101.000	4-632.0	0.29	229.33	129.66	36 44.63	11 48.56	28.76	29.43	28.76	28.97	29.75	28.62	2.775	0.110	0.090	11101
102.000	4-445.0	0.05	457.23	435.27	36 44.63	12 27.44	22.57	22.62	23.39	22.98	23.04	23.65	80.24	5.240	0.329	21111
900.000	4-625.2	0.18	243.12	148.18	36 44.64	11 50.96	99.99	99.99	99.99	26.75	27.00	26.75	5.934	1.053	0.142	01011
103.000	4-625.0	0.09	238.06	145.36	36 44.66	11 50.32	24.33	24.46	25.34	24.72	24.84	25.55	24.01	2.830	0.402	21111
104.000	4-409.0	0.65	497.50	495.00	36 44.69	12 34.78	99.99	99.99	99.99	28.77	28.85	28.79	3.064	1.710	0.083	00000
105.000	4-377.0	0.85	545.50	560.00	36 44.70	12 43.00	99.99	99.99	99.99	28.86	29.42	28.77	2.807	1.006	0.044	01000
106.000	4-603.0	1.19	252.80	170.00	36 44.71	11 53.30	28.53	29.27	28.43	28.64	29.15	28.55	2.591	0.180	0.080	12101
107.000	4-455.0	1.38	402.00	370.50	36 44.71	12 18.74	28.40	28.91	28.23	29.59	29.87	29.71	3.152	0.160	0.095	21101
108.000	4-446.0	0.24	432.33	413.66	36 44.73	12 24.11	28.85	29.49	28.70	99.99	99.99	99.99	2.564	0.110	0.078	20010
109.000	4-579.0	0.14	272.39	199.69	36 44.73	11 56.91	24.97	25.04	25.30	24.98	25.06	25.23	22.51	1.200	0.196	22111
110.000	4-603.0	0.23	256.12	178.75	36 44.74	11 54.24	25.73	25.92	26.35	26.51	26.81	27.01	10.34	1.380	0.234	22111
111.000	4-587.2	0.08	260.16	186.60	36 44.75	11 55.08	28.12	29.01	28.49	29.53	30.23	29.99	3.200	0.070	0.000	10013
112.000	4-340.0	0.10	567.00	598.50	36 44.78	12 47.45	99.99	99.99	99.99	28.31	29.36	28.03	3.978	1.066	0.045	02010
113.000	4-351.0	0.94	539.50	565.00	36 44.80	12 43.00	29.14	29.73	28.82	99.99	99.99	99.99	2.725	0.060	0.051	10001
114.000	4-558.0	0.11	286.32	228.51	36 44.82	12 00.098	22.63	22.66	24.12	22.78	22.85	24.31	50.99	9.250	0.513	22111
115.000	4-422.0	0.66	461.00	461.50	36 44.83	12 29.81	99.99	99.99	99.99	28.78	29.43	28.72	2.599	0.995	0.054	00000
116.000	4-509.0	0.09	329.54	287.77	36 44.84	12 07.569	26.50	26.64	26.78	26.62	26.85	26.95	6.880	0.850	0.178	22111
901.000	4-378.0	1.28	518.30	544.90	36 44.89	12 40.10	99.99	99.99	99.99	25.80	26.71	25.90	23.01	2.364	0.119	00000
117.000	4-455.0	0.04	395.33	382.19	36 44.89	12 19.29	26.56	26.89	26.85	26.87	27.08	26.89	7.612	0.660	0.146	22111
118.000	4-601.0	0.28	222.44	153.11	36 44.91	11 50.07	27.86	28.24	27.92	28.65	29.42	28.44	4.049	0.250	0.127	21101
119.000	4-351.0	0.12	531.10	567.21	36 44.92	12 42.68	26.62	26.90	26.83	28.15	28.69	28.04	9.022	0.450	0.156	22111
120.000	4-423.0	0.09	435.14	441.65	36 44.94	12 26.57	25.37	25.53	26.00	25.66	25.93	26.29	14.34	1.390	0.248	21111
121.000	4-329.0	1.61	540.50	582.00	36 44.94	12 44.44	29.22	29.74	28.78	99.99	99.99	99.99	2.511	0.060	0.052	10001
122.000	4-431.0	0.77	407.66	406.33	36 44.96	12 22.01	28.79	29.53	28.54	99.99	99.99	99.99	3.003	0.090	0.078	10001
123.000	4-607.0	0.21	210.25	144.37	36 44.98	11 48.60	28.08	28.60	28.10	99.99	99.99	99.99	3.614	0.210	0.106	20011
124.000	4-378.0	0.55	509.33	546.02	36 44.99	12 39.67	23.04	23.14	24.86	23.32	23.48	25.24	40.35	7.560	0.573	21101
125.000	4-596.0	0.19	210.30	151.07	36 45.04	11 49.16	26.68	26.92	27.10	26.61	26.78	27.00	6.300	0.740	0.189	21111
126.000	4-515.0	0.11	291.00	259.25	36 45.04	12 02.900	28.67	29.47	28.48	99.99	99.99	99.99	2.768	0.130	0.070	20011
127.000	4-543.0	0.10	261.79	221.36	36 45.05	11 58.01	25.08	25.18	25.81	25.25	25.35	25.92	17.37	1.580	0.272	22111
141.120	4-571.0	0.18	237.26	190.86	36 45.06	11 54.04	23.87	23.98	24.95	24.04	24.16	25.18	48.44	2.500	0.335	21111
128.000	4-431.2	0.04	401.46	412.21	36 45.07	12 22.09	27.47	28.33	27.84	28.38	29.05	28.84	4.400	0.130	0.248	20013
129.000	4-342.0	1.96	487.50	531.00	36 45.12	12 37.09	99.99	99.99	99.99	28.93	29.69	28.48	2.644	0.788	0.000	00000
130.000	4-573.0	0.21	210.38	162.66	36 45.14	11 50.11	26.85	27.05	27.01	28.43	29.04	28.46	5.945	0.630	0.146	22111
131.000	4-530.0	0.17	265.54	236.90	36 45.14	11 59.53	27.69	28.29	27.93	27.67	28.09	27.72	4.457	0.280	0.158	22111
132.000	4-502.0	0.31	300.24	283.82	36 45.17	12 05.454	24.75	24.82	25.75	25.06	25.18	25.96	18.27	2.370	0.318	22101
133.000	4-329.0	0.10	528.70	591.95	36 45.17	12 44.52	26.23	26.45	26.38	26.69	26.97	26.68	10.61	0.630	0.140	22111
134.000	4-456.0	1.03	341.00	350.00	36 45.25	12 13.35	28.34	28.78	28.26	99.99	99.99	99.99	2.920	0.200	0.098	20001

29

TABLE 4—Continued

ID	WFPC	s (arcsec)	x	y	R.A.	Decl.	t_{160}	i_{160}	a_{160}	t_{110}	i_{110}	a_{110}	S/N	A (arcsec²)	r_1 (arcsec)	Tests
135.000......	4-407.0	0.12	412.89	447.69	36 45.26	12 25.69	25.16	25.29	25.86	25.25	25.43	25.94	16.56	1.510	0.261	22111
136.000......	4-593.0	0.30	173.22	129.51	36 45.28	11 45.13	26.20	26.35	26.48	26.07	26.24	26.46	9.240	0.820	0.178	21101
141.112......	4-555.11	0.18	213.18	184.93	36 45.29	11 52.05	23.54	23.92	24.37	24.04	24.49	24.96	106.5	1.080	0.273	22111
137.000......	4-342.0	0.08	486.66	551.11	36 45.30	12 38.64	27.62	27.96	27.57	27.14	27.64	27.09	5.417	0.220	0.105	21111
138.000......	4-498.0	0.11	278.72	274.80	36 45.32	12 03.422	25.99	26.10	26.24	26.44	26.67	26.68	10.51	0.920	0.170	22111
141.100......	4-555.0	0.57	222.83	197.86	36 45.33	11 53.94	20.84	20.92	22.04	21.41	21.48	22.59	170.5	19.86	0.786	22100
141.111......	4-555.0	0.17	224.45	204.37	36 45.34	11 54.37	21.20	21.41	22.04	21.80	22.01	22.59	403.9	4.100	0.296	22111
139.000......	4-395.0	0.04	414.87	460.04	36 45.34	12 26.82	26.39	26.73	26.73	26.15	26.29	26.33	8.580	0.700	0.161	22111
141.110......	4-555.0	0.59	219.17	199.24	36 45.34	11 53.94	20.91	21.02	22.04	21.51	21.63	22.59	259.6	11.01	0.693	22100
140.000......	4-368.0	0.04	455.06	514.43	36 45.35	12 33.74	24.16	24.30	24.98	24.80	24.95	25.44	28.98	2.650	0.283	22111
141.000......	4-555.0	0.66	219.83	199.84	36 45.36	11 53.91	20.71	20.74	22.04	21.51	21.63	22.59	135.4	29.60	0.998	22100
141.112......	4-555.1	0.56	213.08	191.80	36 45.37	11 52.66	22.50	22.71	23.81	23.10	23.31	24.41	143.1	3.290	0.643	21100
142.000......	4-379.0	0.01	438.50	493.00	36 45.37	12 30.99	99.99	99.99	99.99	28.95	29.32	28.47	2.596	1.100	0.049	01010
143.000......	4-407.2	0.71	407.18	453.94	36 45.37	12 25.84	28.83	30.17	29.20	29.04	31.81	29.50	2.800	0.030	0.000	01003
144.000......	4-487.0	0.85	265.50	263.50	36 45.38	12 01.719	99.99	99.99	99.99	28.09	28.86	28.01	3.036	0.565	0.114	01000
145.000......	4-454.0	0.01	332.74	358.70	36 45.41	12 13.54	22.07	22.10	22.35	21.43	21.45	21.68	119.0	5.920	0.206	22111
146.000......	4-467.0	0.04	299.50	313.00	36 45.41	12 07.803	28.57	29.11	28.49	29.42	30.10	29.03	2.698	0.160	0.097	21111
141.112......	4-555.1	0.15	212.64	196.90	36 45.41	11 53.02	23.02	23.41	23.81	23.68	24.14	24.41	163.4	1.160	0.225	21111
147.000......	4-384.2	0.04	418.76	475.17	36 45.42	12 28.29	27.67	28.51	28.04	27.83	28.84	28.29	3.100	0.100	0.000	10013
148.000......	4-557.0	0.23	186.45	163.79	36 45.42	11 48.72	24.45	24.53	25.04	25.16	25.34	25.63	22.87	2.550	0.253	22111
149.000......	4-330.0	0.10	486.00	565.00	36 45.43	12 39.71	28.23	28.45	28.40	99.99	99.99	99.99	3.444	0.180	0.089	20011
150.000......	4-487.0	0.32	263.63	268.88	36 45.45	12 02.021	26.39	26.75	27.70	27.21	27.58	27.76	6.179	1.200	0.452	22101
151.000......	4-582.2	0.50	153.04	125.15	36 45.47	11 43.53	27.73	28.62	28.10	28.71	29.84	29.17	2.700	0.090	0.000	00003
152.000......	4-344.0	0.50	456.00	529.50	36 45.47	12 34.99	28.97	29.63	28.73	99.99	99.99	99.99	2.690	0.080	0.048	10000
153.000......	4-424.0	0.07	346.00	385.00	36 45.49	12 16.49	28.32	28.87	28.19	28.28	28.70	28.18	3.278	0.170	0.069	21111
154.000......	4-487.0	0.08	260.75	270.25	36 45.50	12 01.994	99.99	99.99	99.99	28.09	28.42	28.04	2.760	0.590	0.098	01011
155.000......	4-344.0	0.06	451.68	528.13	36 45.51	12 34.62	26.72	26.99	26.95	26.66	26.99	26.94	6.447	0.670	0.155	22111
156.000......	4-307.0	0.91	493.80	584.40	36 45.51	12 41.81	99.99	99.99	99.99	27.86	28.55	27.80	4.102	0.898	0.100	01000
157.000......	4-330.2	0.73	478.52	569.07	36 45.54	12 39.59	27.25	27.93	27.62	32.21	99.00	32.67	7.700	0.170	0.000	10003
158.000......	4-323.0	1.43	460.75	545.25	36 45.55	12 36.57	28.57	29.38	28.53	99.99	99.99	99.99	2.690	0.160	0.072	20001
159.000......	4-345.0	0.03	442.70	522.20	36 45.56	12 33.57	26.30	26.50	26.50	26.29	26.64	26.51	9.460	0.680	0.149	22111
160.000......	4-323.0	1.15	457.66	542.66	36 45.57	12 36.21	99.99	99.99	99.99	28.51	29.24	28.50	2.806	0.795	0.084	01000
161.000......	4-330.2	1.22	480.06	576.14	36 45.59	12 40.26	27.47	28.30	27.84	29.12	30.32	29.58	4.600	0.110	0.000	10003
162.000......	4-582.2	0.77	149.09	133.67	36 45.59	11 43.99	27.52	27.65	27.89	27.86	28.56	28.32	7.900	0.220	0.000	01003
163.000......	4-389.0	0.09	389.35	456.44	36 45.61	12 24.95	26.02	26.25	26.43	26.60	26.84	26.88	10.85	0.830	0.182	21111
164.000......	4-307.0	0.84	482.88	582.88	36 45.63	12 41.05	99.99	99.99	99.99	27.23	27.72	27.70	4.670	1.067	0.178	01000
165.000......	4-563.0	0.21	140.98	126.03	36 45.63	11 42.86	25.98	26.13	26.62	26.73	27.03	26.94	9.138	1.170	0.305	22111
166.000......	4-307.0	0.16	488.13	592.80	36 45.65	12 42.05	22.24	22.29	22.97	23.37	23.49	24.04	87.28	7.230	0.329	22111
167.000......	4-551.0	0.20	156.00	148.25	36 45.65	11 45.63	99.99	99.99	99.99	28.29	28.92	28.05	3.133	0.795	0.063	01011
141.200......	4-516.0	0.15	203.76	213.36	36 45.66	11 53.83	23.09	23.17	23.65	23.60	23.68	24.08	101.4	2.400	0.243	22111
168.000......	4-563.2	1.27	147.31	139.45	36 45.66	11 44.34	27.56	28.20	27.93	28.50	30.31	28.96	4.100	0.140	0.000	10003
169.000......	4-371.2	0.51	393.15	470.94	36 45.68	12 26.38	29.02	30.73	29.39	99.00	99.00	99.00	3.700	0.020	0.000	00003
170.000......	4-371.2	0.34	395.51	478.78	36 45.72	12 27.16	28.25	29.22	28.62	28.05	29.10	28.51	14.70	0.070	0.000	21003
171.000......	4-323.0	0.08	447.50	547.50	36 45.72	12 35.94	28.78	29.14	28.64	99.99	99.99	99.99	2.593	0.120	0.076	10011
172.000......	4-497.0	0.16	219.01	243.37	36 45.74	11 57.18	25.17	25.27	25.61	25.69	25.89	26.09	17.98	1.310	0.210	21111
173.000......	4-307.0	0.96	484.80	599.60	36 45.75	12 42.50	99.99	99.99	99.99	27.72	28.35	27.71	4.763	1.079	0.087	00000
174.000......	4-478.0	0.18	227.55	259.77	36 45.78	11 59.05	27.96	28.38	27.97	28.08	28.57	28.02	3.761	0.240	0.121	22111
175.000......	4-419.0	0.10	313.16	375.16	36 45.79	12 13.69	27.55	27.90	27.61	27.92	28.37	27.81	5.131	0.270	0.120	22111
176.000......	4-387.0	0.06	365.31	445.42	36 45.79	12 22.62	26.92	27.26	27.23	27.16	27.54	27.42	5.658	0.620	0.163	22111

TABLE 4—Continued

ID	WFPC	s (arcsec)	x	y	R.A.	Decl.	t_{160}	i_{160}	a_{160}	t_{110}	i_{110}	a_{110}	S/N	A (arcsec^2)	r_1 (arcsec)	Tests
177.000......	4-520.0	0.17	175.89	192.10	36 45.80	11 50.38	25.14	25.23	25.52	25.28	25.38	25.56	18.24	1.340	0.199	22111
178.000......	4-307.0	1.18	479.25	599.75	36 45.81	12 42.14	28.33	29.16	28.26	99.99	99.99	99.99	3.509	0.140	0.123	00000
179.000......	4-305.0	0.97	458.25	571.25	36 45.82	12 38.57	99.99	99.99	99.99	28.49	28.69	28.23	2.861	0.987	0.091	01000
180.000......	4-497.0	1.22	208.66	240.33	36 45.83	11 56.33	28.70	28.64	28.87	99.99	99.99	99.99	3.269	0.090	0.100	10000
181.000......	4-305.0	1.40	449.00	561.50	36 45.84	12 37.21	99.99	99.99	99.99	28.69	29.61	28.59	2.810	0.846	0.052	00000
182.000......	4-552.0	0.33	126.30	130.80	36 45.85	11 42.39	99.99	99.99	99.99	27.92	28.28	27.84	2.937	0.573	0.138	01000
183.000......	4-305.0	0.62	451.50	569.50	36 45.88	12 38.02	99.99	99.99	99.99	27.98	28.59	27.66	3.669	0.718	0.121	00000
184.000......	4-473.0	0.08	215.83	256.95	36 45.90	11 58.12	26.80	27.01	27.01	26.48	26.70	26.77	5.773	0.720	0.155	21111
185.000......	4-337.2	0.85	397.48	503.75	36 45.92	12 29.30	28.17	29.48	28.54	99.00	99.00	99.00	11.60	0.060	0.000	10003
186.000......	4-305.0	0.09	449.50	574.54	36 45.94	12 38.31	25.31	25.53	26.02	25.55	25.82	26.10	15.55	1.360	0.249	22111
187.000......	4-326.0	0.03	409.20	521.53	36 45.95	12 31.49	26.97	27.30	27.04	27.01	27.45	27.14	7.849	0.330	0.133	22111
188.000......	4-514.0	0.29	161.04	189.65	36 45.95	11 49.31	25.82	25.89	26.22	25.82	26.01	26.24	10.80	1.140	0.211	22101
189.000......	4-460.0	0.22	230.81	284.67	36 45.96	12 01.307	23.27	23.34	24.24	23.50	23.55	24.41	49.73	4.100	0.348	22111
190.000......	4-391.0	0.07	325.00	415.00	36 46.00	12 17.67	28.71	29.45	28.46	28.35	29.03	28.18	3.240	0.090	0.065	21111
191.000......	4-353.0	0.02	359.12	464.87	36 46.04	12 23.82	27.98	28.42	27.89	28.65	28.91	28.49	4.201	0.190	0.100	22111
192.000......	4-331.2	0.64	379.15	494.44	36 46.05	12 27.44	28.51	30.13	28.88	30.32	99.00	30.78	6.400	0.040	0.000	00003
193.000......	4-331.2	0.78	372.66	489.76	36 46.09	12 26.65	28.00	29.07	28.37	27.69	28.80	28.15	16.80	0.070	0.000	11003
194.000......	4-288.0	0.24	437.00	574.50	36 46.09	12 37.53	99.99	99.99	99.99	28.44	29.31	28.31	3.552	1.118	0.042	00010
902.000......	4-550.0	0.54	103.80	132.53	36 46.13	11 41.17	99.99	99.99	99.99	23.19	24.13	23.71	204.7	16.06	0.150	01000
195.000......	4-331.0	0.09	375.00	497.50	36 46.14	12 27.44	28.89	29.78	28.74	28.94	29.69	29.04	2.933	0.080	0.047	22111
196.000......	4-285.0	0.05	429.46	572.66	36 46.16	12 36.88	27.19	27.51	27.38	99.99	99.99	99.99	6.405	0.330	0.134	20011
197.000......	4-299.0	0.17	416.12	555.75	36 46.16	12 34.67	27.83	28.29	28.03	28.08	28.60	27.89	4.438	0.220	0.155	22111
198.200......	4-522.0	0.21	122.47	163.02	36 46.19	11 44.75	25.09	25.12	25.48	25.32	25.44	25.66	24.42	1.170	0.215	22111
198.100......	4-550.0	0.61	105.23	142.07	36 46.19	11 41.86	19.84	19.87	22.01	20.38	20.45	22.69	292.8	27.98	0.834	22101
198.000......	4-550.0	0.63	106.77	143.04	36 46.19	11 41.88	19.83	19.85	22.01	20.38	20.45	22.69	269.0	31.00	0.862	22101
199.000......	4-294.0	0.21	417.40	560.20	36 46.20	12 35.13	28.25	29.00	28.18	99.99	99.99	99.99	3.718	0.150	0.114	20011
201.100......	4-322.0	0.02	377.44	508.20	36 46.20	12 28.45	23.72	24.38	24.41	24.13	24.67	24.66	108.9	0.690	0.160	22111
200.000......	4-465.0	0.21	181.00	245.50	36 46.21	11 55.04	29.04	30.01	28.93	99.99	99.99	99.99	2.556	0.080	0.046	20011
201.000......	4-322.0	0.35	378.54	512.71	36 46.23	12 28.77	23.32	23.40	24.41	23.60	23.70	24.66	44.67	4.490	0.466	22100
201.200......	4-322.1	0.10	379.72	514.44	36 46.26	12 29.10	24.60	25.25	25.09	24.63	25.17	25.26	53.74	0.590	0.170	22111
202.000......	4-300.0	0.03	403.80	550.05	36 46.27	12 33.49	24.58	24.69	25.17	24.86	24.97	25.26	24.70	1.870	0.238	22111
203.000......	4-341.0	0.03	340.50	466.50	36 46.31	12 22.81	27.41	27.75	27.54	28.65	28.97	28.65	5.139	0.340	0.158	22111
204.000......	4-448.0	0.13	203.91	284.88	36 46.33	11 59.65	24.15	24.28	25.49	24.38	24.53	25.64	23.95	3.600	0.414	22111
205.000......	4-262.0	2.35	436.83	600.00	36 46.36	12 39.56	27.76	28.42	27.72	28.34	29.34	28.05	5.325	0.180	0.120	12100
206.000......	4-322.1	0.99	379.00	525.00	36 46.39	12 29.92	28.92	29.41	28.72	99.99	99.99	99.99	2.634	0.090	0.075	10000
207.000......	4-327.0	0.04	347.32	485.77	36 46.41	12 24.77	25.50	25.66	25.97	25.95	26.13	26.33	14.62	1.110	0.210	22111
208.000......	4-372.0	0.03	292.80	416.45	36 46.43	12 15.80	26.18	26.43	26.69	26.33	26.58	26.76	8.814	0.910	0.202	22111
209.000......	4-418.0	0.34	225.20	328.88	36 46.48	12 04.507	24.19	24.36	25.79	24.45	24.64	25.93	18.89	4.700	0.475	21101
210.000......	4-489.0	0.20	116.93	186.06	36 46.52	11 46.29	27.28	27.59	27.40	99.99	99.99	99.99	5.689	0.350	0.151	20011
211.000......	4-303.0	0.04	359.17	515.47	36 46.55	12 27.93	26.91	27.21	27.12	27.95	28.35	27.85	7.756	0.370	0.139	22111
212.000......	4-471.0	0.18	140.16	227.69	36 46.55	11 51.17	20.89	20.91	21.59	21.31	21.34	21.94	181.9	15.49	0.358	22101
213.000......	4-488.0	0.26	105.41	183.80	36 46.59	11 45.39	25.85	26.00	26.20	26.30	26.75	26.62	11.92	0.900	0.191	22111
214.000......	4-416.0	0.07	208.98	322.61	36 46.60	12 03.023	24.14	24.20	24.71	24.22	24.33	24.76	29.82	2.530	0.258	22111
215.000......	4-350.0	0.02	280.30	422.50	36 46.61	12 15.53	26.42	26.58	26.65	26.75	26.92	26.88	7.997	0.740	0.160	22111
216.000......	4-434.0	0.15	171.40	277.01	36 46.66	11 57.02	25.52	25.63	26.01	25.54	25.71	25.96	14.16	1.140	0.218	21111
217.000......	4-262.0	1.11	405.60	591.70	36 46.66	12 36.98	27.41	27.93	27.48	28.57	29.28	28.45	5.676	0.270	0.112	22100
218.000......	4-412.0	0.18	198.42	315.00	36 46.61	12 01.774	28.29	29.00	28.33	99.99	99.99	99.99	2.843	0.230	0.118	20011
219.000......	4-280.0	0.07	362.00	539.86	36 46.66	12 30.09	27.16	27.45	27.22	27.14	27.55	27.29	6.704	0.320	0.140	22111
220.000......	4-475.0	0.26	102.78	193.91	36 46.66	11 46.06	26.38	26.73	26.72	28.06	28.76	27.48	8.220	0.730	0.159	22101

31

TABLE 4—Continued

ID	WFPC	s (arcsec)	x	y	R.A.	Decl.	t_{160}	i_{160}	a_{160}	t_{110}	i_{110}	a_{110}	S/N	A (arcsec²)	r_1 (arcsec)	Tests
221.000.....	4-411.0	0.12	188.71	309.14	36 46.67	12 00.703	27.90	28.48	27.80	27.75	28.22	27.76	4.679	0.180	0.100	22111
222.000.....	4-442.0	0.20	147.91	255.89	36 46.67	11 53.86	24.75	24.86	25.35	24.94	25.03	25.45	20.65	1.890	0.242	21111
223.000.....	4-488.0	1.38	94.666	185.38	36 46.70	11 44.92	99.99	99.99	99.99	25.72	26.73	26.41	11.76	1.135	0.267	01000
224.000.....	4-475.2	1.16	94.890	189.46	36 46.71	11 45.21	25.24	25.58	26.36	25.39	25.64	26.38	24.50	0.810	0.000	02003
225.000.....	4-336.0	0.02	276.10	432.86	36 46.73	12 16.12	26.14	26.43	26.73	27.59	28.02	27.66	8.661	0.980	0.207	22003
226.000.....	4-334.0	0.04	284.27	444.55	36 46.73	12 17.59	26.68	27.07	27.00	27.02	27.22	27.06	7.052	0.620	0.148	21111
227.000.....	4-241.2	0.07	397.14	599.88	36 46.76	12 37.12	21.80	21.80	22.06	22.25	22.25	22.56	222.9	2.550	0.000	21111
228.000.....	4-388.2	0.06	219.00	361.25	36 46.77	12 06.800	28.69	29.43	28.32	99.99	99.99	99.99	2.702	0.130	0.100	22013
229.000.....	4-241.2	1.84	378.75	575.75	36 46.78	12 34.08	99.99	99.99	99.99	28.57	29.13	28.45	2.533	0.655	0.109	20011
230.000.....	4-432.0	0.12	139.00	258.29	36 46.81	11 53.50	27.43	27.82	27.68	27.85	28.52	28.29	4.724	0.370	0.148	01000
231.000.....	4-382.2	0.10	210.20	355.00	36 46.82	12 05.743	27.76	28.09	27.75	29.24	29.93	28.72	4.405	0.250	0.101	21111
232.000.....	4-360.0	0.07	231.00	383.50	36 46.82	12 09.341	28.10	28.49	28.07	27.96	28.60	27.91	3.227	0.250	0.111	21111
233.000.....	4-241.2	1.28	382.60	586.60	36 46.84	12 35.20	99.99	99.99	99.99	28.09	28.70	28.14	3.062	0.784	0.130	01001
234.000.....	4-216.0	2.25	362.33	565.66	36 46.88	12 32.20	28.82	29.35	28.72	99.99	99.99	99.99	2.623	0.110	0.075	10000
235.000.....	4-289.0	0.06	323.43	519.69	36 46.93	12 26.09	25.05	25.16	25.62	25.36	25.50	25.77	19.06	1.420	0.238	22111
236.000.....	4-295.0	0.19	305.70	497.63	36 46.94	12 23.18	26.44	26.78	27.09	26.33	26.74	27.18	7.534	0.810	0.233	22111
237.000.....	4-382.0	0.08	199.65	356.86	36 46.95	12 05.276	23.92	24.03	24.85	24.06	24.13	24.86	31.74	3.210	0.319	22111
238.000.....	4-415.0	0.18	143.34	288.00	36 47.01	11 56.19	25.63	25.83	26.33	25.70	25.91	26.38	12.36	1.220	0.250	22111
239.000.....	4-266.0	1.40	329.50	541.00	36 47.06	12 28.23	99.99	99.99	99.99	28.89	29.65	28.68	2.730	0.816	0.055	01000
240.000.....	4-332.0	0.13	235.07	419.31	36 47.09	12 12.48	24.90	25.01	25.55	24.86	24.99	25.41	20.56	1.550	0.252	22111
241.000.....	4-335.0	0.02	205.44	393.66	36 47.21	12 08.599	27.75	28.23	27.76	27.52	27.89	27.54	4.587	0.240	0.116	22111
242.000.....	4-332.2	0.00	227.60	425.96	36 47.23	12 12.58	26.26	26.41	26.49	25.95	26.20	26.22	9.082	0.750	0.162	22111
243.000.....	4-385.0	0.11	146.60	318.12	36 47.24	11 58.84	25.91	26.09	26.36	26.08	26.28	26.44	10.61	1.020	0.201	22111
244.000.....	4-232.0	0.08	330.23	569.21	36 47.28	12 30.72	22.43	22.49	23.73	22.57	22.65	23.85	63.81	9.030	0.520	22111
244.100.....	4-232.0	0.06	331.74	570.95	36 47.28	12 30.79	22.45	22.58	23.73	22.60	22.75	23.85	90.37	5.700	0.446	22111
244.200.....	4-232.2	0.10	319.40	558.55	36 47.32	12 28.99	26.58	26.71	26.64	26.86	27.02	26.57	8.191	0.690	0.171	21111
245.000.....	4-298.0	0.11	240.61	455.05	36 47.33	12 15.78	27.14	27.46	27.53	27.62	27.84	27.60	5.890	0.410	0.188	22111
246.000.....	4-356.0	0.14	146.45	338.63	36 47.42	12 00.524	27.39	27.72	27.43	27.58	27.88	27.55	5.822	0.280	0.116	22111
247.000.....	4-319.0	0.10	190.38	402.11	36 47.46	12 08.379	25.98	26.19	26.48	26.03	26.22	26.49	10.11	1.000	0.211	22111
248.000.....	4-356.0	0.96	139.37	335.25	36 47.47	11 59.79	28.13	28.49	28.20	28.10	28.49	28.06	3.572	0.200	0.103	22101
249.000.....	4-315.0	0.11	205.72	425.93	36 47.48	12 11.23	24.57	24.68	25.51	24.86	24.96	25.65	21.26	2.470	0.333	21111
250.000.....	4-291.0	0.04	221.35	449.21	36 47.51	12 14.09	27.21	27.53	27.31	27.61	28.01	27.60	6.248	0.330	0.129	22111
251.000.....	4-346.0	0.09	152.70	358.04	36 47.52	12 02.502	24.15	24.22	25.06	24.16	24.28	25.13	28.41	2.770	0.317	21111
252.000.....	4-386.0	0.16	93.585	287.07	36 47.58	11 53.06	25.85	26.06	26.46	25.79	26.13	26.31	11.27	1.020	0.223	22111
253.000.....	4-182.0	0.22	324.50	599.00	36 47.62	12 32.65	99.99	99.99	99.99	28.22	28.99	28.13	3.510	0.747	0.094	02010
254.000.....	4-182.0	0.50	322.00	599.00	36 47.64	12 32.42	28.23	28.53	28.52	99.99	99.99	99.99	3.527	0.170	0.117	10000
255.000.....	4-301.2	0.13	181.37	414.66	36 47.66	12 08.833	27.74	28.74	28.11	27.48	28.75	27.94	2.600	0.100	0.000	11013
256.000.....	4-283.0	0.09	202.82	442.41	36 47.66	12 12.37	27.12	27.24	27.39	28.04	28.55	28.05	6.265	0.380	0.178	22111
257.000.....	4-231.0	0.11	259.83	519.41	36 47.67	12 22.15	27.62	27.91	27.71	27.75	28.38	27.60	4.838	0.270	0.119	22111
258.000.....	4-308.0	0.10	177.43	409.50	36 47.68	12 08.187	27.09	27.40	27.26	27.66	28.08	27.73	6.808	0.350	0.149	22111
259.000.....	4-247.0	0.04	242.50	497.50	36 47.68	12 19.32	28.65	29.35	28.55	27.65	27.95	27.67	2.939	0.120	0.082	22111
260.000.....	4-297.0	1.65	186.00	436.00	36 47.80	12 10.85	28.77	29.59	28.56	99.99	99.99	99.99	2.764	0.110	0.066	10001
261.000.....	4-212.0	0.16	263.26	542.34	36 47.82	12 24.22	25.67	25.86	26.31	25.88	26.08	26.33	12.63	1.100	0.250	22111
262.000.....	4-267.0	0.17	200.64	458.52	36 47.83	12 13.59	27.53	28.07	27.91	99.99	99.99	99.99	3.752	0.480	0.233	20011
263.000.....	4-304.0	0.65	196.28	454.85	36 47.85	12 13.02	28.38	28.94	28.16	99.99	99.99	99.99	3.108	0.170	0.114	10000
264.000.....	4-304.0	0.10	150.50	395.00	36 47.86	12 05.358	26.25	26.40	26.43	26.53	26.65	26.65	9.461	0.730	0.150	21111
265.000.....	4-174.0	0.05	291.12	586.12	36 47.89	12 29.52	27.64	28.21	27.53	27.57	28.02	27.55	5.606	0.200	0.102	22111
266.000.....	4-212.0	2.51	265.00	565.00	36 48.01	12 26.20	28.76	29.67	28.68	99.99	99.99	99.99	2.771	0.110	0.062	10001
267.000.....	4-314.0	0.16	115.09	364.36	36 48.01	12 00.689	27.56	27.92	27.59	27.79	27.97	27.85	5.461	0.240	0.114	22111
268.000.....	4-187.0	0.12	246.00	549.50	36 48.10	12 23.78	29.05	29.77	28.98	99.99	99.99	99.99	2.514	0.080	0.057	10010

TABLE 4—Continued

ID	WFPC	s (arcsec)	x	y	R.A.	Decl.	t_{160}	i_{160}	a_{160}	t_{110}	i_{110}	a_{110}	S/N	A (arcsec^2)	r_1 (arcsec)	Tests
277.120......	4-260.0	0.08	191.55	480.69	36 48.13	12 14.86	24.11	24.46	24.66	24.13	24.69	24.79	70.33	0.900	0.187	22111
269.000......	4-265.0	0.13	153.00	430.50	36 48.15	12 08.434	99.99	99.99	99.99	28.81	29.88	28.67	2.512	0.660	0.045	01011
270.000......	4-198.0	0.86	234.50	544.00	36 48.18	12 22.62	28.36	29.31	28.23	99.99	99.99	99.99	3.361	0.150	0.116	10000
271.000......	4-170.0	0.78	231.40	543.00	36 48.21	12 22.35	28.48	29.04	28.33	99.99	99.99	99.99	2.914	0.160	0.092	10000
277.100......	4-260.111	0.28	180.49	478.66	36 48.24	12 13.96	21.66	21.73	23.96	21.76	22.05	24.33	94.11	16.80	0.822	22101
277.110......	4-260.111	0.21	179.09	478.29	36 48.25	12 13.85	21.78	22.13	23.96	21.89	22.44	24.33	163.7	7.180	0.596	22111
272.000......	4-135.0	1.42	261.00	586.50	36 48.25	12 27.75	99.99	99.99	99.99	28.74	29.43	28.89	2.684	1.000	0.058	01000
273.000......	4-170.0	0.09	228.62	550.62	36 48.31	12 22.79	28.24	28.55	28.18	27.40	28.05	27.34	3.047	0.220	0.134	21111
274.000......	4-200.0	0.14	192.62	509.51	36 48.37	12 17.25	26.02	26.48	26.66	26.16	26.46	26.50	10.20	0.930	0.200	22111
275.000......	4-237.0	0.05	141.00	446.14	36 48.42	12 08.942	28.00	28.72	27.97	27.93	28.36	27.97	4.022	0.200	0.101	22111
276.000......	4-135.0	0.08	247.14	588.71	36 48.42	12 27.04	27.89	28.28	27.74	27.89	28.27	27.75	4.726	0.180	0.092	22111
277.000......	4-260.111	1.69	175.38	489.09	36 48.42	12 14.76	20.99	21.05	22.92	99.99	99.99	99.99	97.33	32.80	2.054	20000
278.000......	4-228.0	0.02	133.33	445.33	36 48.50	12 08.393	28.63	29.52	28.61	99.99	99.99	99.99	2.985	0.120	0.086	10011
279.000......	4-122.0	0.31	239.09	594.63	36 48.57	12 27.02	26.53	26.88	26.96	26.34	26.68	27.24	9.547	0.470	0.193	22101
280.000......	4-257.0	0.15	101.98	413.78	36 48.59	12 03.902	25.11	25.20	25.47	25.42	25.50	25.62	20.92	1.120	0.198	22111
277.211......	4-186.0	0.09	170.11	509.01	36 48.63	12 15.83	22.04	22.25	22.92	23.09	23.19	23.75	221.6	3.210	0.297	22111
281.000......	4-229.0	0.10	122.44	445.73	36 48.63	12 07.761	25.41	25.52	25.75	25.59	25.76	25.85	16.67	1.040	0.189	22111
277.210......	4-186.0	0.17	170.45	511.07	36 48.63	12 15.91	21.96	22.08	22.92	22.94	23.03	23.75	157.0	6.060	0.393	22111
277.220......	4-186.0	0.19	167.16	507.53	36 48.64	12 15.71	21.83	21.91	22.92	23.09	23.19	23.75	115.6	10.67	0.558	22111
277.220......	4-260.2	0.03	158.51	497.39	36 48.66	12 14.18	24.26	24.37	25.23	24.15	24.44	25.38	38.16	2.090	0.316	21111
282.000......	4-111.0	0.12	228.00	591.00	36 48.68	12 26.09	99.99	99.99	99.99	27.92	28.55	27.69	3.804	0.901	0.103	01010
277.212......	4-169.0	0.08	171.23	519.32	36 48.71	12 16.74	24.79	25.00	25.26	25.19	25.29	25.61	36.20	0.970	0.213	22111
283.000......	4-154.0	0.04	182.16	539.93	36 48.76	12 19.10	25.29	25.40	25.97	25.48	25.64	26.12	16.37	1.290	0.260	22111
284.000......	4-183.0	0.08	135.00	487.50	36 48.85	12 11.93	28.71	29.32	28.38	99.99	99.99	99.99	2.784	0.120	0.082	20011
285.000......	4-128.0	0.13	182.09	554.36	36 48.89	12 20.25	27.85	28.30	28.07	99.99	99.99	99.99	3.647	0.300	0.148	20011
286.000......	4-199.0	0.08	113.28	464.00	36 48.91	12 08.736	99.99	99.99	99.99	27.98	28.42	27.88	3.431	0.734	0.099	02011
287.000......	4-148.0	0.14	160.00	527.80	36 48.92	12 16.78	99.99	99.99	99.99	28.30	28.81	28.13	2.761	0.705	0.083	01010
288.100......	4-203.0	0.11	107.58	459.56	36 48.92	12 07.981	25.11	25.49	25.84	25.68	25.81	25.94	23.16	1.060	0.208	22111
288.000......	4-203.0	0.26	107.33	461.59	36 48.94	12 08.077	24.86	25.08	25.84	25.68	25.81	25.94	15.47	2.610	0.369	22101
288.200......	4-203.12	0.16	103.06	465.25	36 49.03	12 08.160	26.61	27.00	26.82	27.91	28.54	27.99	11.42	0.340	0.138	20011
289.000......	4-120.0	0.57	178.11	570.54	36 49.06	12 21.28	21.84	21.87	23.29	22.02	22.05	23.50	111.5	8.500	0.464	22101
290.000......	4-99.0	0.13	159.08	569.75	36 49.29	12 20.10	27.52	28.06	27.75	28.10	28.69	28.02	4.911	0.310	0.170	22111
291.000......	4-119.0	2.05	102.00	494.50	36 49.30	12 10.52	99.99	99.99	99.99	28.44	29.49	28.23	3.552	0.942	0.051	00000
292.000......	4-131.0	0.18	123.72	527.72	36 49.34	12 14.53	24.56	24.70	25.43	24.64	24.76	25.52	22.78	2.200	0.291	22111
293.000......	4-74.0	0.34	163.08	596.20	36 49.47	12 22.49	26.59	26.96	27.21	28.36	28.97	28.15	6.479	0.830	0.223	22101
294.000......	4-119.0	0.03	99.500	515.75	36 49.51	12 12.04	27.79	28.29	27.84	27.42	27.74	27.16	4.707	0.210	0.121	22111
295.100......	4-85.0	0.09	146.10	580.31	36 49.52	12 20.14	23.87	24.04	24.66	24.02	24.13	24.74	55.24	1.680	0.278	22111
295.000......	4-85.0	0.48	141.71	581.26	36 49.58	12 20.01	23.40	23.48	24.66	99.99	99.99	99.99	40.72	4.620	0.591	20000
296.000......	4-109.0	0.11	98.397	524.45	36 49.61	12 12.70	24.37	24.43	24.75	24.95	25.01	25.19	34.17	1.500	0.209	21111
297.000......	4-100.0	0.12	106.00	535.50	36 49.61	12 14.06	29.01	29.99	28.84	99.99	99.99	99.99	2.617	0.080	0.046	20011
298.000......	4-95.0	0.15	112.50	545.18	36 49.62	12 15.27	27.05	27.32	27.17	27.75	28.01	27.66	7.161	0.340	0.138	22111
295.200......	4-85.2	0.12	135.60	583.23	36 49.68	12 19.76	24.54	24.71	25.10	25.11	25.24	25.48	35.91	1.270	0.222	21111
299.000......	4-50.2	0.65	98.680	564.65	36 49.94	12 15.98	27.56	28.92	27.93	99.00	30.37	99.00	2.500	0.070	0.000	10003
300.000......	4-50.0	0.65	101.50	571.00	36 49.97	12 16.68	29.13	29.76	28.76	99.99	99.99	99.99	2.695	0.060	0.059	00000
302.200......	4-50.0	0.15	96.083	570.75	36 50.03	12 16.33	27.14	27.18	26.67	27.26	27.45	27.58	7.245	0.330	0.140	12111
301.000......	4-33.2	0.48	95.890	584.44	36 50.15	12 17.42	21.76	21.76	22.70	22.34	22.34	23.23	301.0	3.830	0.000	22003
302.000......	4-33.0	0.13	94.419	581.94	36 50.17	12 17.05	20.97	21.00	22.18	21.68	21.68	22.78	200.0	10.17	0.473	22110
302.100......	4-33.0	0.14	93.381	582.58	36 50.17	12 17.05	20.97	21.02	22.18	21.68	21.68	22.78	222.0	8.970	0.459	22110
303.000......	4-33.0	1.25	93.600	592.20	36 50.26	12 17.97	99.99	99.99	99.99	27.85	28.38	27.76	4.187	1.046	0.086	00000

NOTE.—Units of right ascension are minutes and seconds, and units of declination are arcminutes and arcseconds.

33

that filter. The F160W and F110W objects are considered to be in common if they lie within 0″.25 of each other. If the last digit in the tests parameter (see below) is 3, the magnitudes are from the SExtractor procedure.

S/N.—The signal-to-noise ratio value quoted in the catalog is calculated by the same technique used in the optical HDF. The value of the signal-to-noise is $S/N = L_i/\sigma(L_i)$, where the variance $[\Gamma\sigma(L_i)]^2$ is

$$[\Gamma\sigma(L_i)]^2 = \Gamma N_{obj} + 1.9^2\Gamma^2\sigma_{sky}^2 A_{obj} + 1.9^2\Gamma^2\sigma_{sky}^2 A_{obj}^2/A_{sky}$$
(2)

as quoted in its correct form by Pozzetti et al. (1998). For NICMOS, the value of Γ in electrons per ADU is 6.5. L_i is the sky-subtracted number of counts, σ_{sky} is the sky sigma in ADUs, and the object and sky areas A_{sky} and A_{obj} are the areas in pixels returned by KFOCAS. This equation reformulated in terms of count rates in ADUs s^{-1} is given by

$$\sigma_{tot}^2 = rate_{obj}/(\Gamma t) + 1.9^2\sigma_{skyrate}^2 A_{obj} + 1.9^2\sigma_{skyrate}^2 A_{obj}^2/A_{sky} .$$
(3)

Here $rate_{obj}$ is the sky-subtracted source count rate in ADUs s^{-1}, $\sigma_{skyrate}$ is the sky sigma value in ADUs s^{-1}, and t is the integration time in seconds. The final signal-to-noise ratio is $rate_{obj}/\sigma_{tot}$. The measured value of the sky sigma is 2.2×10^{-4} ADUs s^{-1} for the F160W image and 2.5×10^{-4} for F110W as shown in Figure 2. The factor of 1.9 in each of the equations is the estimated value of the noise correlation discussed earlier. Figure 9 shows a plot of the signal-to-noise ratios calculated by this method for the KFOCAS determined sources.

A.—This is the isophotal area of the source in square arcseconds as determined from the value returned by KFOCAS.

r_1.—This is the half-light radius returned by KFOCAS.

$Tests$.—This parameter indicates which of the various reliability tests the source passed. A source that passed all tests has a value of 22111, one that passed no tests has a value of 00000. The first number is 0, 1, or 2 if the source was detected in none, one, or both of the F160W half-catalogs. For an explanation of the half-catalogs see § 10.1. The second number is the same test in the F110W catalog. The third number is 0 or 1 depending on whether the source was found in both NICMOS bands of the full image extrac-

tions. The fourth number is 0 or 1 depending on whether the source is detected in the WFPC2 catalog. The last number is 0 or 1 depending on whether the source was found in the independent Sextractor catalog. Note the discussions in §§ 10.2 and 10.3 on the differences in half-catalog detection probabilities between KFOCAS and SExtractor. In all cases a common detection means that the source centroids lie within 0″.25 of each other. No color or magnitude tests are applied as part of the common object association.

9. COMPLETENESS

Our calculated 50% completeness levels are KFOCAS AB aperture magnitudes of 28.7 and 28.2 for point objects and extended sources in the F160W filter and KFOCAS AB magnitudes of 28.6 and 28.0, respectively, in the F110W filter. These limits are based on a technique of adding sources to the image at various flux levels and running the source extraction programs to see what percentage of the added sources are recovered. These numbers are based on the KFOCAS reductions.

9.1. KFOCAS Completeness

The test for the KFOCAS program established a regular grid of 49 positions in a 7×7 pattern that evenly covered the image area utilized in the catalog extraction. Sources are placed at these positions to create a new image that contains the original image plus the added sources. KFOCAS then creates a new catalog utilizing exactly the same parameters used in the final catalog preparation. An automatic program checks the new catalog to see what percentage of the added sources are recovered by KFOCAS. The sources are sequentially dimmed in half-magnitude steps from their original magnitudes of about 21 to the final magnitude of 32. The added sources are real sources extracted from the final image. The NICMOS source 145, the central star, represents a point object and the elliptical galaxy, NICMOS 212, is the extended object. These are WFPC2 sources 4-454 and 4-471, respectively. Alteration of the position of the grid confirmed that the completeness limits were consistent at different grid positions. The extended source completeness limit will of course be brighter for more extended objects than NICMOS 212, but this galaxy is one of the largest in the image.

The completeness value at a given magnitude is for the magnitude of the input source, not the magnitude at which the source is recovered. This value is approximately equal to the recovered magnitude for sources brighter than 26.5. At the very faintest levels, the recovered magnitudes are 0.3–0.5 mag fainter than the input magnitudes. The measured completeness limits are fitted by

$$\left(1 - \frac{m - m_b}{m_a - m_b}\right)^n \sqrt{\frac{m_b}{m}} .$$
(4)

In this function m_a is the magnitude at which the completeness goes to zero, m_b is the magnitude at which the completeness is 100%, and the power index n is adjusted to fit the data. The function is purely empirical, simply designed to fit the data well. This function smooths the curves and provides the interpolation from the observed magnitudes to the magnitudes used in Table 5. As expected from the nonuniform quality map of the image, the completeness limit is not uniform over the image. The comple-
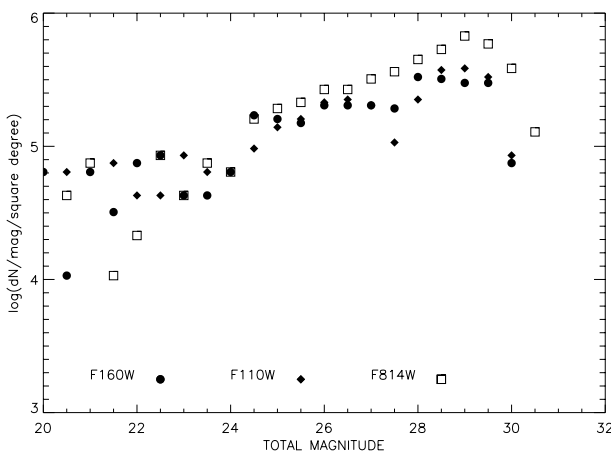

FIG. 9.—Signal-to-noise ratios for faint sources relative to the KFOCAS aperture magnitudes for the F160W and F110W filters. This figure contains all of the extracted sources, not just the catalog sources.

ness is somewhat lower in the right-hand half of the image. The completeness limits in Table 5 should be considered as an average across the image.

9.2. *SExtractor Completeness*

For the SExtractor catalog we used an analysis similar to the one described in Yan et al. (1998). We selected a compact galaxy (4-289 in the Williams catalog), representative of the majority of the objects in our field, and dimmed it in half-magnitude increments from 25.5 to 29. The dimmed galaxy was dropped at random positions 10,000 times, superposed on the full image and two images with half the exposure time of the full image. (The "half-" images are discussed in § 10.1.) We ran SExtractor at the position at which the galaxy was dropped at each iteration to determine whether or not the dimmed galaxy was recovered and at what magnitude. The use of random positions in the simulations allows us to include completeness corrections arising from nondetections and magnitude errors caused by crowding and spatially dependent errors in the sky subtraction and flat-field correction. As discussed in § 9.1, the completeness values for recovery of the images are again an area average of the completeness since the sensitivity across the NICMOS images is not uniform. These same experiments also give us the matrix relating the input and output aperture magnitudes for those galaxies that are recovered. The input magnitude and mean recovered magnitude agree to within 0.07 mag in the bins through 28. At 28.5 the mean of the recovered galaxy magnitudes begins to brighten (28.21), and by an input magnitude of 29 it brightens substantially (28.11). The galaxies that land on negative noise regions are lost completely. The SExtractor catalog becomes 50% complete at AB ≈ 28.3 for the compact galaxies in our survey.

To test differences in detectability of the point-spread function due to the source landing at different locations within the 0″2 pixels, we ran incompleteness tests using the central star (NICMOS 145, AB = 22.1) taken from five different individual exposures, all taken at different dither positions. These have only 1/120 the exposure time of the final image and therefore have lower signal-to-noise ratios. We found no substantial differences in detection rates, other than as the star is dimmed to AB = 28, it is missed most frequently in the upper right-hand quadrant of the detector, the least sensitive region of the image. In the final combined image, we found no obvious location dependence. We detect the star 95% of the time as it is dimmed to AB = 27, and then the detection rate drops rapidly to 50% complete at AB = 28.5.

10. SOURCE RELIABILITY TESTS

Even though the listed catalog does not contain objects with signal-to-noise ratios less than 2.5, there can be false detection still in the catalog. As indicated in § 8, the catalog indicates the degree of coincidence between the various subcatalogs that make up the total catalog. These data are provided as an aid in discerning the reality of the sources. Any statistical study of these results should utilize the test flag indices of Table 4 carefully along with the completeness and reliability results discussed here and in § 9 and summarized in Table 5. See § 10.4 for a discussion of this table. Table 6 presents a catalog of detected sources with signal-to-noise ratios less than 2.5.

TABLE 5
COMPLETENESS AND RELIABILITY

		KFOCAS						SX		
MAGNITUDE[a] (1)	S/N (2)	Cs_{16} (3)	Cl_{16} (4)	Cs_{11} (5)	Cl_{11} (6)	R_{16} (7)	R_{11} (8)	C_{16} (9)	$R_{co\,16}$[b] (10)	$R_{neg\,16}$[c] (11)
20.000	283.8	100.0	100.0	100.0	100.0	1.000	1.000	...	...	...
20.500	287.9	100.0	100.0	100.0	100.0	1.000	0.833	...	...	...
21.000	166.5	100.0	100.0	100.0	100.0	1.000	0.750	...	...	...
21.500	195.8	100.0	100.0	100.0	100.0	1.000	0.750	...	...	...
22.000	114.2	100.0	98.85	100.0	100.0	1.000	0.800	...	...	...
22.500	125.0	100.0	97.75	100.0	98.88	1.000	0.900	...	...	...
23.000	79.12	100.0	96.67	100.0	97.79	1.000	0.875	...	...	...
23.500	48.68	98.93	95.62	98.93	96.71	1.000	0.542	...	...	...
24.000	58.21	97.89	94.53	97.89	95.58	1.000	0.916	...	...	...
24.500	28.31	96.87	93.35	96.87	94.28	1.000	0.663	...	...	...
25.000	22.32	95.83	91.91	95.83	92.63	0.961	0.732	...	...	...
25.500	17.82	94.66	90.01	94.66	90.36	1.000	0.783	97.6	...	...
26.000	12.59	93.14	87.31	93.14	87.11	0.973	0.806	96.2	...	...
26.500	9.327	90.89	83.32	90.89	82.42	0.957	0.722	95.1	...	...
27.000	7.192	87.28	77.38	87.28	75.68	0.977	0.601	92.2	...	...
27.500	5.989	81.38	68.62	81.38	66.17	0.848	0.610	89.1	...	...
28.000	4.852	71.85	55.91	71.85	53.01	0.681	0.458	76.6	0.94	0.87
28.500	3.580	56.86	37.82	56.86	35.17	0.461	0.205	41.5	0.68	0.50
29.000	2.889	33.96	12.57	33.96	11.44	0.247	0.122	14.1	...	...
29.500	2.260	0.000	0.000	0.000	0.000	0.157	0.075	...	...	...
30.000	1.635	0.000	0.000	0.000	0.000	0.123	0.079	...	...	...

NOTE.—The brighter magnitude bins in the SExtractor columns have no measurements as no tests were run at these values. The completeness and reliability are assumed to be very high for AB < 26.5 as shown in the KFOCAS tests.

[a] For the KFOCAS columns the values refer to the magnitudes measured by KFOCAS. For the SExtractor columns the values refer to the magnitudes measured by SExtractor.

[b] $R_{co\,16}$ refers to the full coincidence formalism described in § 10.1.1.

[c] $R_{neg\,16}$ refers to the negative image technique described in § 10.1.2.

TABLE 6

CATALOG OF DETECTED SOURCES WITH SIGNAL-TO-NOISE RATIO LEVELS LESS THAN 2.5

ID [a]	WFPC	s (arcsec)	x	y	R.A.	Decl.	t_{160}	i_{160}	a_{160}	t_{110}	i_{110}	a_{110}	S/N	A (arcsec^2)	r_1 (arcsec)	Tests
501.000......	4-851.0	0.53	557.50	139.00	36 40.88	12 09.423	29.98	29.85	30.34	99.99	99.99	99.99	1.255	0.060	0.051	20000
502.000......	4-807.0	0.15	561.00	170.50	36 41.11	12 12.19	29.35	30.28	29.02	28.28	28.79	28.19	1.917	0.080	0.050	20111
503.000......	4-822.0	1.01	543.50	151.00	36 41.15	12 09.547	29.99	29.89	29.69	99.99	99.99	99.99	1.240	0.060	0.051	10000
504.000......	4-822.2	1.47	538.16	149.94	36 41.19	12 09.121	27.82	30.29	28.19	99.00	99.00	99.00	0.900	0.020	0.000	00003
505.000......	4-807.0	1.71	559.33	188.16	36 41.28	12 13.54	28.64	28.82	28.64	99.99	99.99	99.99	2.365	0.180	0.119	20000
506.000......	4-766.0	1.00	562.50	197.00	36 41.33	12 14.49	99.99	99.99	99.99	29.14	30.00	29.14	2.146	0.592	0.050	01000

NOTE.—Table 6 is presented in its entirety in the electronic edition of the Astronomical Journal. A portion is shown here for guidance regarding its form and content. Units of right ascension are minutes and seconds, and units of declination are arcminutes and arcseconds.

[a] Sources with signal-to-noise ratio levels less than 2.5 have ID numbers of 500 or greater.

10.1. Half-Data Reductions

Our primary test of the reliability of observed sources utilizes two independent images formed from subsets of the integrations in each filter. The two images contain the even- and odd-numbered integrations from a sequential numbering of the integrations after removal of images with excess cosmic-ray persistence. Since there are three images per orbit, this technique ensures that orbits are mixed between the groups and that each group has an equal mix of images observed at different times during the orbit. The widths of the histograms of pixel values in the half-images are a factor of $\sqrt{2}$ wider than the full image histograms. This is a good indication that the width of the histogram in Figure 5 is due to noise rather than faint sources.

These half-data reductions are the primary tests as they represent truly independent sets of data that measure the same quantity. Although useful, the coincidences between the KFOCAS and SExtractor catalogs are not measurements of two independent data sets. The coincidences between the objects detected in the various NICMOS and WFPC2 filter sets are again useful, but they are not measuring the same quantity. As with the completeness tests, the checks on the KFOCAS and Sextractor image catalogs are carried out independently. With slight modifications, however, the logic of the tests is essentially identical.

10.1.1. Logic of the Half-Catalog Tests

Our goal is a measurement of the probability that a detected source with a given magnitude range is real. To facilitate the comparison between KFOCAS and SExtractor tests, we utilized 0″.6 diameter aperture magnitudes in both source extraction programs. We start by grouping sources into half-magnitude bins centered on integer and half-magnitudes. Our analysis method then utilizes the statistics of objects detected in both, only one, or neither of the independent half-catalogs for each aperture magnitude bin. We consider objects as being present in both catalogs if their centroids are within 0″.25 (2.5 drizzled pixels) of each other.

From the completeness studies described in § 9 we determined the probability $P_{A,B}(j, k)$ that an object in a magnitude bin j is recovered in a bin k where A or B refers to one of the half-catalogs. The completeness is then $C_A(j) = \sum_k P_A(j, k)$ and similarly for image B. Let $N_R(j)$ be the number of real objects whose true magnitudes lie within bin j. In addition, due to noise fluctuations (both Poisson and nonrandom), there will be some false objects detected in bin j. Let $f_A(j)$ be the probability that any object in image A in bin j is a false detection, and let $N_A(j)$ be the number of

objects found in bin j on image A. Then

$$N_A(j) = \sum_k N_R(k) \times P_A(k, j) + f_A(j) \times N_A(j) ; \quad (5)$$

and

$$N_B(j) = \sum_k N_R(k) \times P_B(k, j) + f_B(j) \times N_B(j) . \quad (6)$$

We then count the number of objects $N_{AB}(i, j)$ that appear in common in both half-images A and B (i.e., which agree in position to within 0″.25 of each other) and that have measured magnitudes in A that place them in bin i and measured magnitudes in B that place them in bin j. Then

$$N_{AB}(i, j) = \sum_k N_R(k) \times P_A(k, i) \times P_B(k, j) . \quad (7)$$

Strictly speaking, we should add to equation (7) a term that represents the number of times that a false detection in both half-images will be coincident to within 0″.25 and will land in the two magnitude bins in question. In practice this number is small compared to one, and we neglect it.

If N_{bins} is the number of magnitude bins, then equations (5) and (6) hold for the N_{bins} values of j and in equation (7) for the $N_{bins} \times N_{bins}$ combinations of i and j. The unknown quantities are the N_{bins} values for the number of real sources with true flux placing them in bin $N_R(k)$ along with the N_{bins} estimates for the probabilities $f_A(j)$ and $f_B(j)$ that a given source in bin j is not a real source. Obviously, the system is overdetermined. This is to be expected since equations (5), (6), and (7) are just discrete representations of integral equations describing the observed number count distribution from which we are trying to recover the true distribution, taking into account losses, false sources, and errors between the true and measured magnitudes due to noise.

A simplification of the preceding equations that is useful for illustrative purposes and actual calculations in some cases comes from ignoring the cross-terms and letting the completeness in any bin be equal to C independent of which half-catalog is addressed. This eliminates the cross terms in equations (5), (6), and (7).

In that case, we obtain for each bin,

$$N_R = N_{AB}/C^2 \quad (8)$$

and

$$f_A = 1 - N_{AB}/(C \times N_A) ; \quad (9)$$

with a similar expression for f_B.

10.1.2. Negative Image Tests

As described below, we are limited in the applicability of the full formalism described above owing to small number

statistics in the observed number of objects, which can lead to reliability estimates greater than 1. An alternative procedure is to multiply the final images by -1.0 and search for "detections" of objects in these negative images. This assumes that the noise properties of the images are the same for negative excursions as for positive ones. This is not in general true since, for example, cosmic rays that are not completely removed have no counterpart in the negative image. In the case of the NICMOS HDF images, however, not only are the cosmic rays removed fairly effectively within each frame as a consequence of the nondestructive readout but the very large number of dithered frames making up our final images also reduces any residual cosmic rays by a further larger factor. Unfortunately, we have found that this method does not appear to be well suited for the KFOCAS extractions for reasons associated with edge effects near the large negative "holes" in the counts produced by the bright real sources in the negative images. However, this method does seem to yield useful results for the SExtractor algorithm. We now discuss the particular tests actually carried out on the KFOCAS and SExtractor half-catalogs.

10.2. KFOCAS Half-Catalog Tests

The KFOCAS analysis of each half-image used the same parameters as the total image analysis. Since the images are in units of photon flux, the half-images have the same signal strength for true sources but have a higher noise. Unlike SExtractor, the 1 σ noise level for KFOCAS is an input parameter. Retention of whole catalog input parameters results in an input 1 σ noise value that is a $\sqrt{2}$ lower than the noise in the half-catalog. The half-image KFOCAS analysis then detects more sources, since more random noise fluctuations appear above the detection threshold. Bright true sources should be detected in both images. Faint sources of course could be detected in only one or even neither of the half-images. Each source is marked in the catalog test column as to whether it appeared in both, only one, or none of the half-images.

In practice for the KFOCAS source we utilize the simplified formalism described in equations (8) and (9) of § 10.1.1. In particular we note that the reliability in either half-catalog is $1 - f_A$ or $1 - f_B$, so we can say that the reliability r is

$$r_A = N_{AB}/(C \times N_A) . \tag{10}$$

Since all of the quantities on the right-hand side of equation (10) are known, r can be calculated using the values of C previously determined. However, when this is formally carried out, the values of r for some magnitude bins become greater than 1 owing to a low value of C for that bin or small number statistics. Since the true value of the completeness can never exceed one we can get a robust lower limit on r by setting C equal to 1 and noting that

$$r_A \geq N_{AB}/N_A \tag{11}$$

with again a similar equation for r_B. This equation depends solely on the ratio of the number of sources detected in both catalogs to the number detected in one of the half-catalogs. The final reliability for a magnitude bin is just the average of f_A and f_B. This reliability is appropriate for the half-catalogs. The signal-to-noise ratio in the whole catalog is a factor of $\sqrt{2}$ higher. This corresponds the objects in the

half-catalog that are the same factor brighter. This is an offset of 0.376 mag; therefore, the calculated reliability numbers in the half-catalog are appropriate for sources that are 0.376 mag fainter in the whole catalog.

Table 5 contains the results of these tests under the section marked KFOCAS. The completeness values listed in the table are the values found from the analysis in § 9.1. The reliability numbers are the numbers from the above calculation adjusted to the appropriate aperture magnitude for the total catalog. These values are in general lower than those calculated using the measured values for completeness in equation (10).

10.3. Sextractor Half-Catalog Tests

For both the whole image and half-images, we use the SExtractor parameters given in Table 3 but determine the completeness independently for the half-images using the same procedure described in § 9.

As noted above, the noise properties in the half-images scale almost exactly as expected, so that the false detection rate at a given magnitude bin in the half-images should be applied to a magnitude bin in the whole image fainter by $1/\sqrt{2}$ lower in the flux, or 0.376 mag. We then use the mean of the two false detection rates determined from the half-images for the estimate of the false detection rate at this slightly fainter magnitude.

As described in § 10.1.1, the system of equations (5)–(7) for $N_R(k)$ is overdetermined, and we determined these values by a least-squares fit to the observed values $N_{AB}(i, j)$. Equations (5) and (6) then give the false detection rates for the two half-images and use the mean of these determinations for the whole image as explained above.

In practice, as already discussed in § 10.2, the small number of sources actually detected in common in the two half-images results in uncertainties in the reliability estimates for magnitudes at which the completeness is near unity. We have also estimated the reliability of the detections by the negative image method described in § 10.1.2. The objects that SExtractor finds using this technique do not seem to occur preferentially near the "holes" associated with the negative sources but occur in the higher signal-to-noise ratio regions, as expected, so that SExtractor does not seem subject to the same degree to the edge effects described in § 10.1.2 for KFOCAS.

10.4. The Completeness and Reliability Table

The completeness and reliability table, Table 5, summarizes the results of our tests described above. Columns (2)–(8) refer to the KFOCAS reductions only, and columns (9)–(11) refer to the results from SExtractor. As described in § 7.4, there is a systematic difference between aperture magnitudes measured by KFOCAS and SExtractor, which becomes significant for objects fainter than ≈ 28.0, as shown in Figure 8. Thus, in the first column, the magnitude is the aperture AB magnitude measured by KFOCAS for the KFOCAS reductions and by SExtractor for the SExtractor reductions. The width of the magnitude bin is 0.5 mag centered on the value in the magnitude column. The signal to noise ratio (S/N) is the average signal-to-noise ratio for all objects in the magnitude bin. The columns labeled Cs_{16}, Cl_{16}, Cs_{11}, and Cl_{11} are the completeness numbers for the KFOCAS reduction listed in order for small and large objects in the F160W filter and the F110W filter, respectively. Next are the reliability numbers for the F160W and

F110W filters, where no discrimination has been made between small and large objects. Completeness and reliability SExtractor results for the F160W filter comprise the last three columns, where the column labeled $R_{co\,16}$ uses the full half-image formalism, while the column labeled $R_{neg\,16}$ uses the negative image technique. It should be emphasized that the reliability estimates at the faint end of the table are subject to considerable uncertainty. However, the results all seem to indicate a fairly low incidence of false detections $\sim 5\%-15\%$ at magnitude ~ 27.5, but this incidence rises steeply at fainter magnitudes, while the completeness is of order $\sim 80\%-90\%$ at magnitude 27.5, of order $\sim 70\%-75\%$ at magnitude 28.0, and falls rapidly beyond that point. KFOCAS appears to lose more objects owing to merging with other objects than SExtractor particularly for bright objects. This is probably the cause of the less than 100% completeness at bright magnitudes for the KFOCAS reductions. The low number of objects in the brighter bins limits the accuracy of the measurements, and differences of $\pm 5\%$ should not be considered significant.

Our discussion of the differences in source extractions in § 7.4 clearly indicates that the IDL and IRAF images are essentially identical and that the magnitude differences in Figure 8 are due solely to differences between the two extraction programs, KFOCAS and SExtractor. There are also differences in the number of detections between the two programs. Running SExtractor on the IDL image with the same set of parameters used for the SExtractor analysis of the IRAF images, we find 284 galaxies, somewhat less than the 356 found on the IRAF image. On the other hand, there are a total of 350 objects selected by KFOCAS from the whole IDL F160W image, also more than those found by SExtractor on the IDL image. The total number of objects found in the F160W image by KFOCAS and in the IRAF image by SExtractor is nearly identical.

Inspection of Table 5 indicates the range of reliability and completeness measures returned by the two methods. In general the reliability and completeness measures from the KFOCAS analysis fall below those determined via the SExtractor analysis. This is particularly true when one considers the difference in faint magnitudes discussed in § 7.4. This indicates that at the faintest magnitudes the KFOCAS numbers should be compared with the SExtractor numbers for sources with SExtractor magnitudes nearly a magnitude brighter than the KFOCAS magnitude. Part of this difference in reliability is due to the KFOCAS numbers being lower limits on the reliability as discussed in § 10.2. Another part of the difference, however, is due to the uncertainty inherent in these calculations, and users of this catalog should be aware of them. Our net philosophy is to be aggressive in identifying potential sources but to be relatively conservative in calculating their reliability and completeness.

11. GALAXY COUNTS

As with the original optical catalog of Williams et al. (1996), it is not our intention in this paper to discuss scientific results. A commonly used statistic, however, is the differential number count of galaxies. Figure 10 presents this statistic for the region of the HDF covered by our catalog. The galaxy counts in number per magnitude per square degree have been divided into half-magnitude bins. If the object radius is less than $0\rlap{.}''3$, the aperture magnitude is used. If the object radius is greater than this, the isophotal
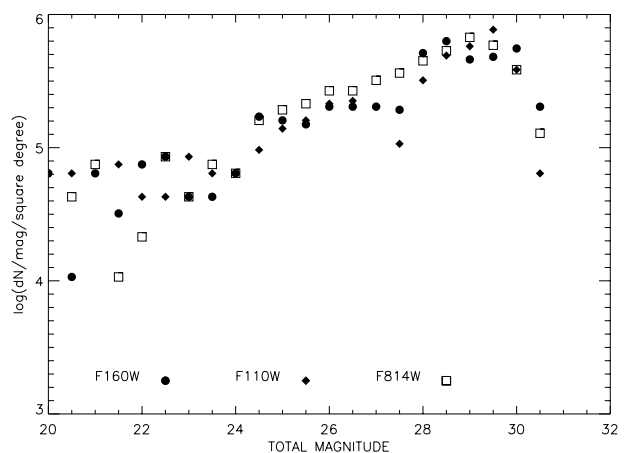

FIG. 10.—Differential galaxy counts as a function of AB aperture magnitude only of the sources appearing in the sigma-limited catalog.

magnitude is used. The number counts for the F814W filter in the same area as determined from the optical catalog are also shown for comparison. The same division between aperture and isophotal magnitudes are used for the F814W data. The counts for the WFPC2 F814W objects includes all of the WFPC2 catalog objects in the NICMOS field, not just those in common with NICMOS objects. There are no aperture corrections applied to this data in order to facilitate comparison with the statistics presented in Williams et al. (1996). It should be noted that the area covered by the NICMOS image is very small. For a value of $H_0 = 50$ and a value of $\Omega_0 = 1$, the sides of the NICMOS image are on the order of 250 kpc for redshifts greater than 1. This is about 10 times smaller that the typical diameter of a region forming a single galaxy from cold dark latter simulations (Steinmetz 1998). Drawing any cosmological conclusions from this small sample may be very suspect. Following the discussion in Williams et al. (1996) we have not eliminated split objects from the number counts. Except at very bright magnitudes, we do not expect this to affect the statistics significantly.

12. CONCLUSIONS

The NICMOS observations of the Hubble Deep Field add significant value to the existing data by providing improved wavelength coverage and access to objects that are either too heavily extincted or too highly redshifted to be visible in the original optical catalog. This paper is designed to be a reference source for the use of this data in various areas of research. Future papers will discuss various aspects of the significance of these data.

REFERENCES

Bertin, E., & Arnouts, S. 1996, A&A, 117, 393
Connolly, A. J., Szalay, A. S., Dickinson, M., SubbaRao, M. U., & Brunner, R. J. 1997, ApJ, 486, L11
Dickinson, M., et al. 1997, *HST* Approved Cycle 7 Observing Plan
Fruchter, A. S., & Hook, R. N. 1997, Proc. SPIE, 3164, 120
Fruchter, A., Hook, R. N., Busko, C., & Mutchler, M. 1997, in The 1997 *HST* Calibration Workshop, ed. S. Casertano, R. Jedrzejewski, C. D. Keyes, & M. Stevens (Baltimore, MD: STScI), 518
Jarvis, J. F., & Tyson, J. A. 1981, AJ, 86, 476
Lehar, J., Falco, E. E., Impey, C. D., Kochanek, C. S., McLeod, B. A., Munoz, J., & Rix, H.-W. 1999, in preparation
McLeod, B. 1997, in The 1997 *HST* Calibration Workshop, ed. S. Casertano, R. Jedrzejewski, C. D. Keyes, & M. Stevens (Baltimore, MD: STScI), 281

Pozzetti, L., Madau, P., Zamorani, G., Ferguson, H. C., & Bruzual A., G. 1998, MNRAS, 298, 1133
Steinmetz, M. 1998, in Space Telescope Symposium on the Hubble Deep Field, in press
Valdes, F. 1982, Faint Object Classification and Analysis System (KPNO Internal Publication)
Williams, R. E., et al. 1996, AJ, 112, 1335.
Yan, L., McCarthy, P. J., Storrie-Lombardi, L. J., & Weymann, R. J. 1998, ApJ, 503, L19